Building a Watershed Information System for the Campo de Cartagena basin (Spain) integrating hydrological modeling and remote sensing

June 2014

Authors:
S. Contreras
J.E. Hunink
A. Baille

Commissioned by
European Commission FP7
Universidad Politécnica de Cartagena, Spain

Report FutureWater: 125

FutureWater
Paseo Alfonso XIII, 48
30203 Cartagena (Murcia)
España

+34 868 071 286

info@futurewater.es

www.futurewater.es

Preface

A good understanding of the water balance of semiarid Medtiranean basins and good access to this information by water managers is necessary for the assessment and implementation of water management policies and measures, taking into account the environmental impacts. Also for the Campo de Cartagena basin, southeastern Spain, an integrated picture of the water balance (flows and stocks) is lacking. Regional data on irrigation water use is not available and surface-groundwater interactions have not been assessed through a basin-wide modelling approach.

Satellites provide us with an increasing amount of spatially-distributed data which is strongly related with the hydrological functioning of our natural and agro- ecosystems. Also, Geografic Information Systems and web mapping tools offer an efficient way for integrating data from remote sensing within hydrological modelling tools and making this information accessible to end-users. Together, these tools can provide a powerful framework for solving a large number of questions related with the monitoring and management of our water resources.

This report summarizes the development of a decision support tool for the Campo de Cartagena basin integrating hydrological modelling and remote sensing data. The resulting Watershed Information System of Campo de Cartagena (WIS-CT) shows synthetic and quantitative outputs of the different water balance components at the catchment scale. This report provides a detailed description of all the development stages and describes how satellite data is combined with the hydrological model SPHY (*Spatial Processes in Hydrology*), for estimating the water balance of this particular region. This work was carried out within the project "*Sustainable use of irrigation water in the Mediterranean Region*" (SIRRIMED, www.sirrimed.org). SIRRIMED is an international project funded by the European Commission under the EFP7 Cooperation Theme "*Food, Fisheries and Biotechnologies*".

Table of contents

Tables

Figures

1 Introduction

1.1 Background

Imbalances between water supply and demand and competition among different water sectors are increasing in many water-stressed basins in the world. However, in many cases, decision makers in the water sector lack good access to information on the basin scale where important decisions need to be made and a complete picture of the basins status is necessary. This information needs to be coherent and harmonized in order to provide an integrated picture useful for the assessment of the problems. Normally, many relevant hydrological data are available to obtain this picture but the information is scattered and not implemented in a single, consistent framework.

The goal of the SIRRIMED project (www.sirrimed.org) was to develop and test techniques and decision support tools for the three primary scale levels: plot, district and watershed. These tools should support more sustainable irrigation management in the Mediterranean region. On the watershed scale, the goal was to develop a so-called Watershed Information System (WIS).

A WIS is a tool that supplies synthetic and quantitative outputs of the different water balance components at the catchment scale. A WIS should provide insight in how different irrigation schemes influence the spatial patterns of water use, and their potential effects on the quantity and quality of the downstream water resources.

In short, the WIS has the following goals:

a) quantify the spatial patterns of water use, irrigation requirements by crops, and returning flows in terms of potential recharge into aquifers
b) evaluate the hydrological effects of irrigation activities at the watershed scale, and
c) improve the regional planning of water resources

The development of an information system at the watershed level is a prerequisite for identifying, and for proposing strategies of water management compatible with the environmental constrains of semiarid Mediterranean regions.

1.2 Content of this report

This report describes the modelling structure adopted for the WIS of the Campo de Cartagena Basin (WIS-CT) and the different stages followed for its implementation. The key elements and modules of the WIS-CT are detailed, the input datasets, and the output directed to the regional stakeholders. For the WIS-CT, a water accounting approach was used [*Molden and Sakthivadivel*, 1999; e.g. *Karimi et al.*, 2013].

The specific objectives covered by the WIS-CT include:

a) Apply a hydrological model to assess the water balance for the 2000-2012 period.

b) the integration of the water balances into a water accounting framework

c) the development of a web-platform which makes the spatial data available to potential end-users (water users and stakeholders).

This report is divided in four sections. The *Material and Methods* section describes the water-balance model used in the WIS-CT, the collection and processing of the input data, the calibration/validation procedures, the analyses performed for testing the sensitivity of the water-balance model, and the meteorological forcing inputs used to evaluate the potential impacts that climate change may impress on the water accounts of the region. In the third section, results from the sensitivity analysis are presented, and the water accounts at the basin scale resulting from different model configurations are analyzed for the present meteorological conditions and several future climate scenarios. Finally, in the fourth section, the online web visualization is presented, in which the most relevant spatial datasets reported in this study have been uploaded.

2 Material and Methods

2.1 Study area

Campo de Cartagena basin is located at SE Spain, in the Murcia region (Figure 1). It covers a predominantly flat area with an acreage of 1218 km^2 and comprises 35 subcatchments, with sizes ranging from 0.2 km^2 up to 696 km^2, all of them drainining to the Mar Menor lagoon. The NW and SW borders of the basin fit with mountainous areas of low altitude (highest point at 1071 m a.s.l.), while the Mar Menor and the Mediterranean Sea are located at the East. The basin has an average altitude of 151 m a.s.l. and it is characterized by its gentle slope which averages 7.5%. Climate is semiarid with a strong Mediterranean regime. Mean annual precipitation is 300 mm, and mean annual temperature ranges from 14ºC to 17ºC. Potential evapotranspiration averages 1275 mm/y. For a more detailed description of the area see [*Jiménez-Martínez et al.*, 2009; *Baudron et al.*, 2013].

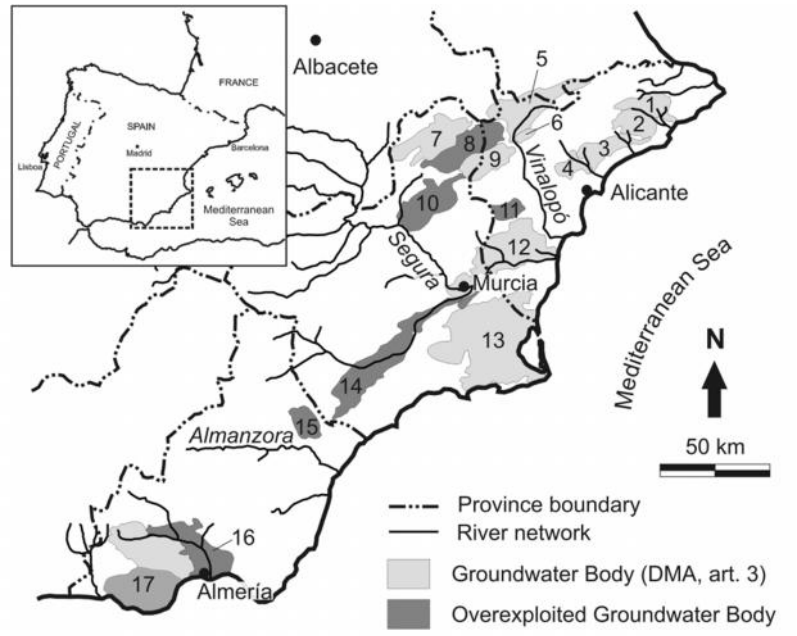

Figure 1. Map location of the Campo de Cartagena study area (it covers approximately the groundwater body num. 13).

Land use distribution (Figure 2) in Campo de Cartagena is extremely heterogeneous. Based on the SIOSE geodatabase (www.siose.es), the study are is mainly occupoed by by a compound-moisaic cover class which integrates an irregular and heterogenous pattern of different land use classes. After, the most important homogeneous classes are herbaceous (horticulture-row) crops and Citrus orchards (Figure 3) (a brief description of the SIOSE project is given by [*Perez-Hoyos et al.*, 2014].

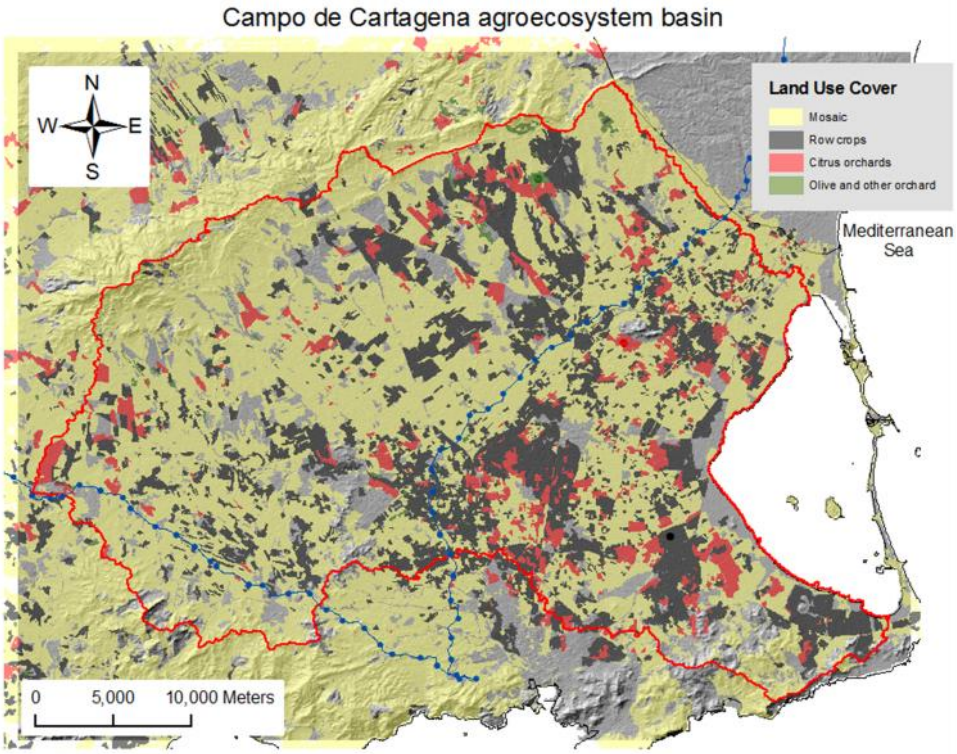

Figure 2. Main Land Use Cover types in the Campo de Cartagena basin. Dots show the pixel locations used to retrieve NDVI average trajectories.

According the agro-statistics reported by the regional government, agriculture acreage in the basin reached 32.366 ha. In 2011 horticulture-row crops were the main crop type in the farmland area (65% of coverage). Citrus orchards (lemon, orange, mandarine and grapefruits) covered more than 8.250 has (Figure 3). In plots dominated by row crops, rotation of autumn-winter (e.g. lettuce, artichoke) and spring-summer (e.g. melon) crops is a very common practice. Drip irrigation is the main irrigation system in the study region.

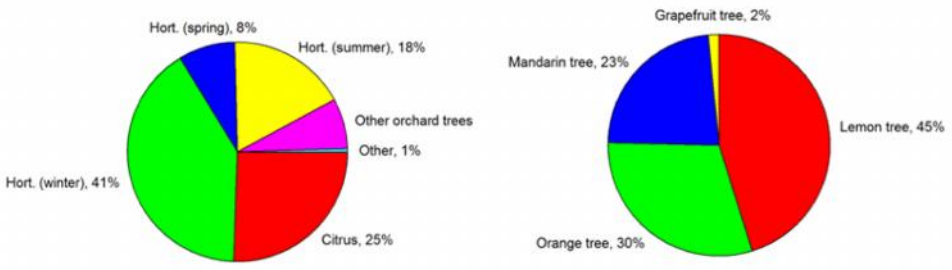

Figure 3. Percentage of row crops and orchard trees in Campo de Cartagena basin in 2011.

Irrigation in the basin is distributed in four zones (Figure 4), three of which are under the management of the Campo de Cartagena Irrigation Community (CCIC). The fourth area is outside the CCIC and was defined from the irrigation zone units used in the River Water Management Plan of the Segura River Basin by the Segura Basin Water Authority.

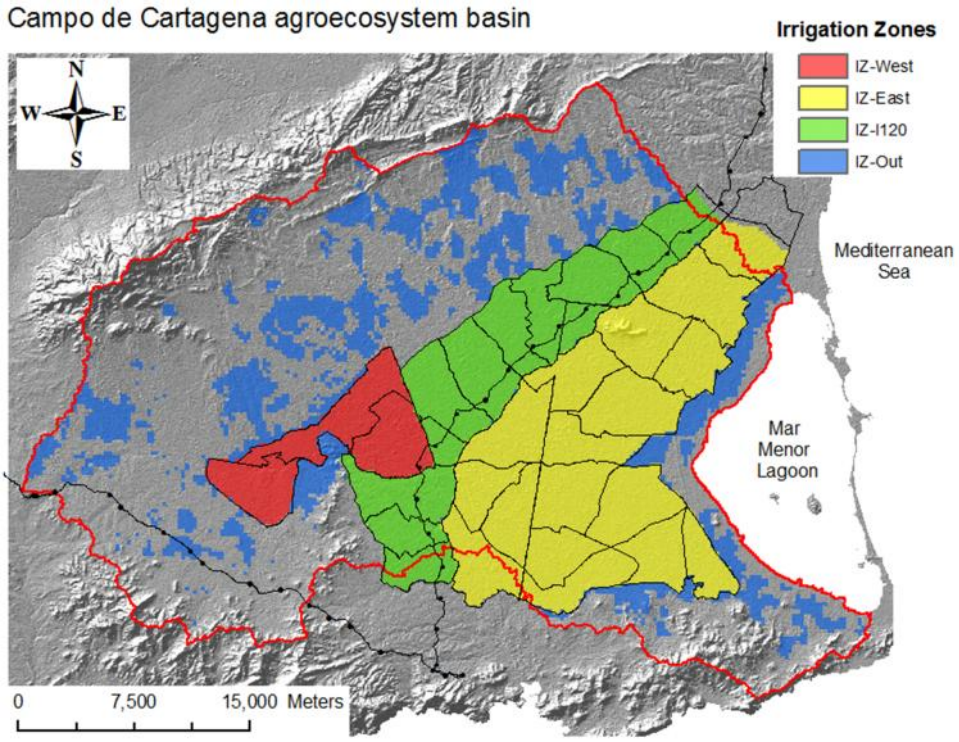

Figure 4. Irrigated zones in Campo de Cartagena basin. IZ-West = western irrigation zone; IZ-East = eastern irrigation zone; IZ-I120 = irrigation zone along the level 120 m.; IZ-Out additional irrigation units defined by the Segura Basin Water Authority.

The hydrogeology of the Campo de Cartagena plain consists of a multi-layer complex aquifer (Figure 5) with four sedimentary layers lay over the basement. The upper unconfined aquifer is the most relevant from the point of view of this study because it receives most of the return flows from irrigation. The upper aquifer extends over 1.135 km^2 and comprises Quaternary detrital sediments (mainly sands and silts) [*Jiménez-Martínez et al.*, 2012]. Average thickness is around 50 m and the water table is 15 m. in depth. At the present this aquifer is barely exploited because their waters are polluted by the agrochemicals supplied by the irrigation return flows Jiménez-Martínez et al. [2010].

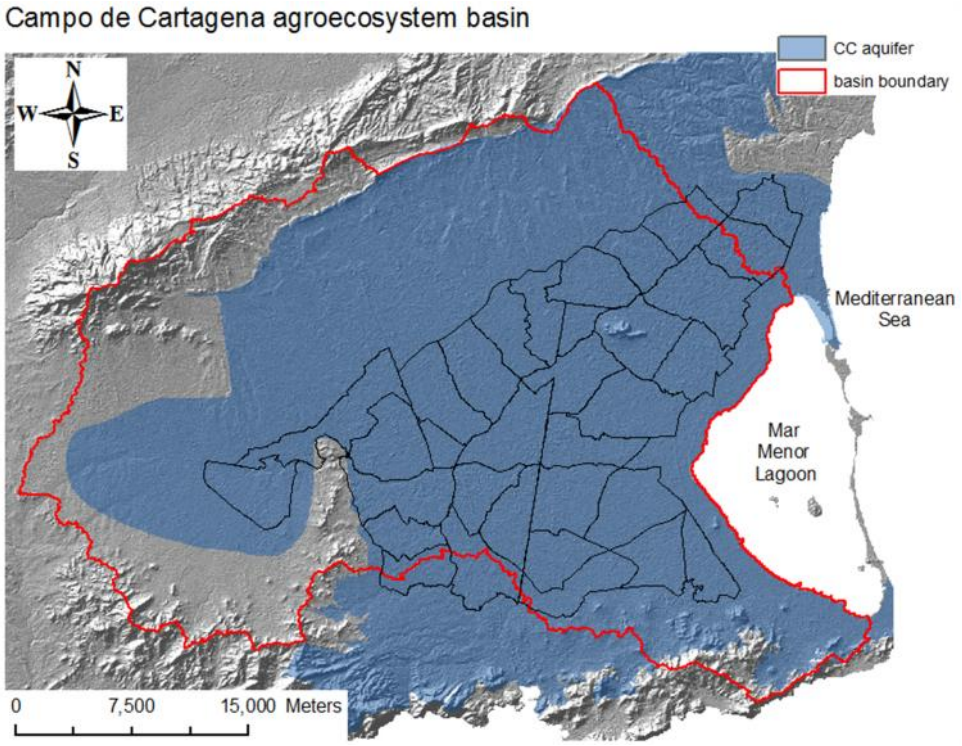

Figure 5. Campo de Cartagena groundwater body.

2.2 SPHY - Conceptual approach

The WIS-CT is based on a soil-water balance model which has been designed to cover the specific objectives of the SIRRIMED project. The water balance model is built upon the SPHY (*Spatial Processes in Hydrology*) model [*Terink et al.*, 2012]. For the WIS-CT, SPHY has been properly adapted to include a satellite-based algorithm for retrieving: a) actual evapotranspiration rates, b) totals of water provided by irrigation, and c) estimates of potential recharge to aquifers.

SPHY for the WIS-CT is based on a pixel-by-pixel monthly soil bucket-water balance approach which simulates the soil water dynamics in the root zone based on the conservation mass equation (Equation 1)

$$Z\frac{d\,s(t)}{dt} = I\left[t, s(t)\right] - O\left[s(t), NDVI(t)\right]$$

Equation 1

where, t = time; Z = soil bucket depth representing the root zone or the active soil depth affected by evapotranspiration losses (mm); s = relative soil moisture content ($0 \le s(t) \le 1$); I[t,s(t)] = rate of water inputs reaching the soil bucket; O[s(t), NDVI(t)] = rate of water losses resulting from the soil bucket. All processes which control the soil water dynamics in the soil bucket depend on the temporal dynamics of the NDVI (Normalized Difference Vegetation Index), the active soil depth (Z), and three key soil parameters, por (porosity), s_{fc} and s_{wp}, which determine its "total storage capacity" (S_{sat} = Z*por), the total soil moisture content retained at the field capacity point (S_{fc} = Z*s_{fc}), and the total soil moisture content retained at the wilting point (S_{wp} = Z*s_{wp}). These parameters define three hydraulic domains (Figure 6) from which losses of water from the soil bucket take place through the mechanisms of surface runoff (rof), evapotranspiration (eta) or

deep drainage (per). S_{sat} determines the threshold above which soil is considered to be fully saturated: any additional supply of water, either by precipitation (pre) or irrigation (irr), above this threshold would promote the generation of surface runoff (saturation-excess runoff mechanism). Percolation (potential recharge in transit) to deeper soil layers as consequence of gravitational forces takes place preferentially through fractures or cracks (per_{pref}) or diffusely when the relative soil moisture content ranges between s_{sat} and s_{fc} (pre_{diff}). In this last case, the rate of diffuse percolation will be exponentially controlled by the saturated hydraulic conductivity (K_{sat}) and the relative soil moisture content. Finally, losses by evapotranspiration (eta) take place according the potential/reference evapotranspiration (etr) and whenever relative soil moisture is higher than s_{wp}. In general, all soil input parameters used in SPHY, i.e. s_{sat}, s_{fc}, s_{wp} and K_{sat} can be computed from soil texture data, and organic matter when is available, using pedotransfer functions (see review by Wösten et al. [2001])

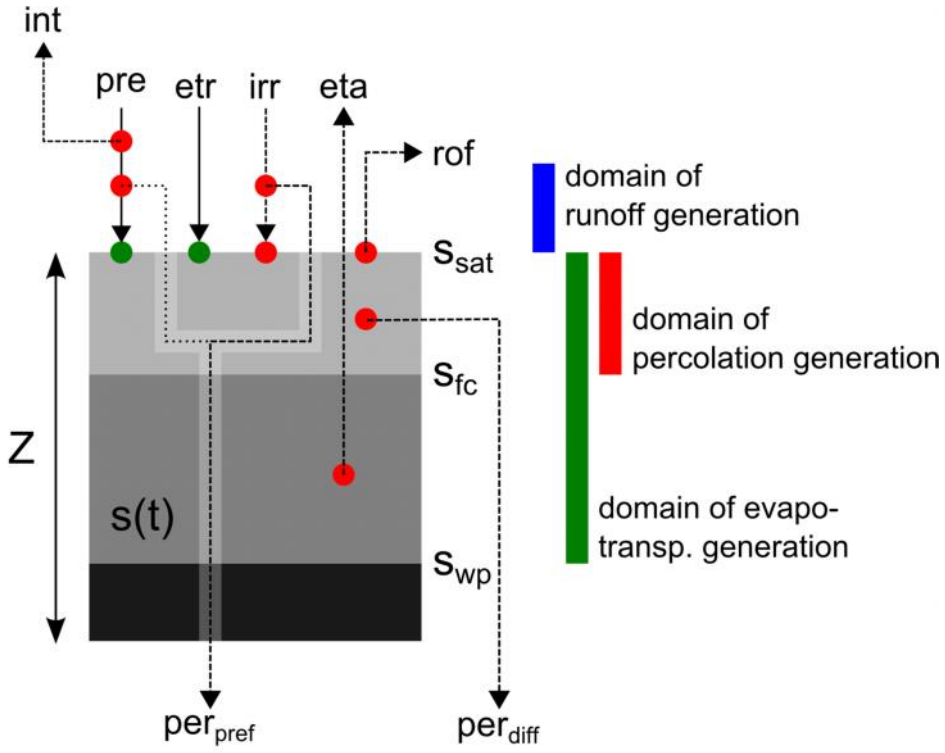

Figure 6. Soil-water bucket model (SPHY) used in this study. Input and outputs variables are shown as green (solid line) and red (dashed lines) circles, respectively.

Precipitation and water supplies from irrigation comprise the main inputs to the soil bucket, as

$$I = pre + irr$$

Equation 2

In which *pre* = precipitation; *irr* = irrigation. In opposite to *pre* which is a user-defined input variable, *irr* is an unknown input variable to the soil bucket but which is afterwards computed based on the relative contribution of the soil moisture to the total evapotranspiration.

Interception, surface runoff, actual evapotranspiration and deep percolation constitute the main losses of water from the soil-water bucket

O = *int* + *rof* + *eta* + *per*

Equation 3

2.2.1 Interception and surface runoff losses

Before reaching the surface, water loss by interception is retrieved at each timestep from the gross precipitation, *pre*, according a user-defined coefficient, *α*, and the Fractional Vegetation Cover (*FVC*) (Equation 4).

$$int = pre \cdot \sim \cdot FVC$$

Equation 4

FVC refers to the ratio of vegetation occupying an unit area. It is computed scaling the observed NDVI between two threshold conditions which represent a fully-vegetated area and a bare soil one [*Carlson and Riziley*, 1997], as

$$FVC = \left(\frac{NDVI - NDVI_{\min}}{p \cdot NDVI_{\max} - NDVI_{\min}} \right)^{¥}$$

Equation 5

In Equation 5, parameter *y* controls the shape of the FCV function and it commonly takes values between 1 and 2. Finally *p*, which takes values from 0 to 1, is a "tolerance" parameter which is additionally included here to relax the maximum NDVI required to assume a full vegetation coverage. Because of its simplicity and the low number of parameters involved, this simple approach is preferred here against another ones, as the Rutter bucket-type model [*Muzylo et al.*, 2009], which require a more complex parameterization.

After the withdrawal of the interception losses, the remaining precipitation reaches the surface and is directly added to the soil bucket to increase the antecedent water content in the soil active zone. If the resulting water content overpasses the total capacity of the soil bucket (S_{sat}), a saturation-excess runoff flux (*rof*) is then computed as

$$rof = \max\left[0, \left(S_{t-1} + pre - int\right) - S_{sat}\right]$$

Equation 6

At its present form, the soil-water balance model here described does not include the infiltration-excess (Horton) mechanism of runoff generation. In semiarid environments with a high recurrence of short and intense rainfall events, the Horton runoff mechanism can reach a great relevance [*Cantón et al.*, 2011]. In general, the relative contribution of each runoff mechanism (saturation-excess vs infiltration-excess) will depend on physical (e.g. lithology, slope) and spatial-scale properties (spatial length). However, the quantification of the Hortonian-type runoff is strongly demanding of high-resolution (hourly-daily) meteorological data and soil ancillary data which is not always available. By the other hand, it is highlighted in scientific literature that as the temporal resolution and the spatial length increase from daily to monthly, and from few to various hundreds of meters, as it has been adopted in this study, saturation-excess mechanism takes increasingly more relevance than the Hortonian-type mechanism [*Descroix et al.*, 2007].

Under these circumstances, the surface runoff generated during intense rainfall events could be more likely re-infiltrated along the path length, making almost negligible the Horton-type runoff against the saturation-type one.

2.2.2 Evapotranspiration losses: the VI-CC approach

Evapotranspiration is estimated using a VI-based crop coefficient approach (hereafter, the VI-CC approach) [*Contreras et al.*, 2011; *Glenn et al.*, 2011; *Kamble et al.*, 2013]. The VI-CC approach combines observations of green foliage density by a satellite-based vegetation index (VI) with meteorological data to estimate evaporation from transpiring vegetation. VIs measure the density of green foliage based on the reflectance of visible and near infrared (NIR) light from the canopy, and are highly correlated with plant physiological processes that depend on light absorption by a canopy such as ET and photosynthesis, and thus the crop coefficient.

Crop coefficient estimation from VIs for irrigation purposes has been broadly studied in herbaceous crops [*Er-Raki et al.*, 2007; *Jayanthi et al.*, 2007; *González-Dugo and Mateos*, 2008; *Sánchez et al.*, 2012] and in woody crops [*Samani et al.*, 2009]. VI-based crop coefficient estimates for natural vegetation have been provided by [*Groeneveld et al.*, 2007; *Campos et al.*, 2013]. Gleen et al. [2011] provides a review of this approach and the relationships between both variables. The primary advantage of VI methods for estimating ET is that transpiration is closely related to radiation absorbed by the plant canopy, which is also closely related to VIs. Hoewever, the main disadvantage is that VIs cannot capture the short-term stress effects on vegetation and the soil evaporation component. Consequently, this approach is useful when is applied in areas where soil evaporation is a minor component of the water balance, and a monthly-annual time scale is adopted.

As it has been stated, the VI-based crop coefficient uses an observed vegetation index, here the NDVI, as a direct surrogate of the stress factors which affect the vegetation/crop performance and, finally, the evapotranspiration coefficient. Then, multiplied by the reference evapotranspiration, the effective evapotranspiration coefficient can be directly and easily converted into rates of actual evapotranspiration. Despite its apparent simplicity, not an universal VI-k_c exits and consequently a vegetation/crop-dependent calibration is rather required. The soil-water balance approach adopted for the WIS-CT uses a simple linear parameterization for the VI-K_c relationship in which the minimum values for the crop coefficient ($k_{c,min}$) are reached in bare soils, and the maximum ones ($k_{c,max}$) are expected to be reached when vegetation/crop is growing at its optimum agronomic condition, i.e. when the NDVI is close to the maximum value observed for a non-stressed coverage. Using the conceptual scheme proposed by FAO-56 [*Allen et al.*, 1998], actual evapotranspiration is estimated as

$$eta = etr \cdot k_{c-VI}$$

Equation 7

in which,

$$k_{c-VI} = \min\left[1,\ \mathrm{k_{c,max}},\ \mathrm{k_{c,min}} + \left(\mathrm{k_{c,max}} - \mathrm{k_{c,min}}\right)\cdot\left(\frac{NDVI - \mathrm{NDVI_{min}}}{\mathrm{NDVI_{max}} - \mathrm{NDVI_{min}}}\right)\right]$$

Equation 8

being *etr* the reference evapotranspiration in depth of water (e.g. mm), $k_{c,min}$ is the bare-soil evaporative coefficient at $NDVI_{min}$, and $k_{c,max}$ is the maximum vegetation/crop coefficient reached at $NDVI_{max}$.

2.2.3 Computing irrigation requirements: fractioning actual evapotranspiration

The soil-water balance model for the WIS-CT assumes a contextual domain in which the irrigation inputs to crops are unknown. In non-irrigated areas, evapotranspiration is exclusively met by the soil moisture retained in the active-rooted zone (eta^{sm}). In irrigated areas, irrigation inputs are computed afterward eta^{sm} is known. Here, eta^{sm} is proportional to a dynamically soil moisture-stress coefficient, *ς*, estimated as

$$¸\left[s(t),t\right]=\min\left[1,\frac{s-s_{wp}}{s_{fc}-s_{wp}}\right]$$

Equation 9

where *s* is the relative soil moisture content at the soil bucket at time t, and s_{wp} and s_{fc} are the values for the relative soil moisture content at the wilting point and the field capacity conditions, respectively.

Finally,

$$eta^{sm}=etr\cdot k_{c-VI}\cdot ¸\left[s(t),t\right]$$

Equation 10

and

$$eta^{irr}=eta-eta^{sm}$$

Assuming an irrigation efficiency at the field/plot scale, irrigation inputs at the pixel level are finally computed as:

$$irr=\max\left[0,\ eta^{irr}/£_{irr}\right]$$

Equation 11

ε_{irr} is a plot-scale coefficient which informs about the efficiency of application, i.e. the fraction of the total water input supplied by irrigation which is not effectively diverted as evapotranspiration loss. It can take vales close to 0 (minimum efficiency in the application, most of the water is lost through percolation) up to 1 (all the water supplied is available for crops).

2.2.4 Deep percolation losses

Two mechanisms of deep percolation generation are considered (Figure 6). Preferential flows from the topsoil (per_{pref} in Figure 6) represents a “fast” route of water loss through soil fractures or cracks, or due to inefficiencies of application during the irrigation practices. To account these losses a user-defined coefficient is adopted (in case of irrigated areas, the application efficiencies at the field/plot scale may be used). By the other hand, the “slow” percolation from the bottom of soil bucket, or the diffuse percolation component (per_{diff} in Figure 6), depends on

the soil moisture content and the saturated hydraulic conductivity [*Laio et al.*, 2001; *Kendy et al.*, 2003].

$$per = per_{pref} + per_{diff}$$

Equation 12

where

$$per_{pref} = (pre - int) \cdot £_{inf} + Irr \cdot (1 - £_{irr})$$

Equation 13

$$per_{diff} = \min\left[(S - S_{fc}),\ K_{sat} \cdot \frac{e^{(s - s_{fc})} - 1}{e^{(por - s_{fc})} - 1} \right]$$

Equation 14

being S the water depth stored in the soil bucket after subtraction of the evapotranspiration losses, s the relative soil moisture content (S/Z) in the soil bucket, and s_{fc} the relative soil moisture content at field capacity. In Equation 13, preferential percolation can be separated in two terms, i.e. a percolation fraction which is generated by the presence of soil fractures or cracks after rainfall reaches the surface, or a percolation which is originated by irrigation inefficiencies. Equation 14 has been proposed by [*Laio et al.*, 2001] and it assumes that the hydraulic conductivity decays exponentially from K_{sat} at s=por (the effective soil porosity), to 0 at $s=s_{fc}$. The parameter β is a power-law coefficient which depends on the type of soil, and ranges from 12 for sandy and homogeneous soils, up to 26 for clayed and heterogeneous ones. The sensitivity of the exponential function to the range of values for the β coefficient is shown in Figure 7. In general the function shows that the more sandy a soil (high β values), the higher the diffuse percolation, and the lower the soil moisture.

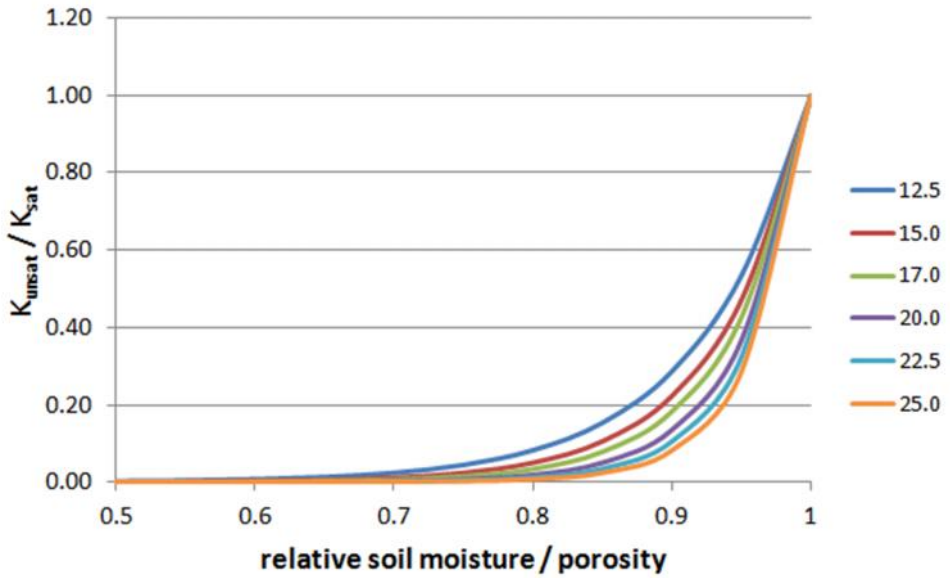

Figure 7. Sensitivity of the diffuse percolation function against values of the betha parameter.

2.2.5 List of variables and parameters

In Table 1 and Table 2 are listed the input variables and parameters required by SPHY and the output variables simulated from it, respectively.

Table 1. Input and output variables involved in SPHY.

Input variables		Output variables	
pre	precipitation	**fvc**	fractional vegetation cover
rad	direct radiation	**kcr**	effective crop coefficient
tmp	mean temperature	**int**	rainfall interception
tmx	mean maximum temperature	**rof**	Hortonian surface runoff
tmn	mean minimum temperature	**eta**	actual evapotranspiration
etr	reference evapotranspiration[1]	**irr**	Irrigation
ndv	satellite-based greenness index[2]	**per**	deep percolation (per_{diff} + per_{pref})
		dra	drainage (rof + per)
		smi	soil moisture at initial of each time step
		smc	soil moisture change at each time step

[1] retrieved from rad, tmp, tmx and tmn

[2] NDVI (Normalized Difference Vegetation Index)

Table 2. Input parameters required by SPHY.

Soil parameters		Vegetation-crop parameters		Other parameters	
DEM	Digital Elevation Model	$NDVI_{max}$	maximum greenness index at FVC=1	ε_{inf}	scalar for rainfall-preferential flow
por	soil porosity	$NDVI_{min}$	minimum greenness index for bare soil	ε_{irr}	irrigation efficiency at the field scale
s_{fc}	soil moisture at field capacity (3 atm)	$K_{c,min}$	maximum crop coefficient		
s_{wp}	soil moisture at wilting point (15 atm)	$K_{c,max}$	maximum crop coefficient		
Z	active soil depth	p	tolerance scalar for VI_{max}		
K_{sat}	Saturated hydraulic conductivity	γ	shape-scalar for the FVC function		
β	percolation - exponential scalar	α	rainfall interception coefficient		

2.3 Input data collection and processing

2.3.1 Precipitation

2.3.1.1 Data collection and gap filling

Monthly precipitation data was collected for the October/2000 – September/2012 period from all the meteorological stations in the study region. The local meteorological network comprises stations managed by the Segura Basin Authority (CHS), the Regional Ministry of Agriculture (SIAM) and the Spanish Meteorological Agency (AEMET) (see Table 3).

Table 3. Meteorological stations at Campo de Cartagena Basin.

Source	ID Station	Name	XUTM	YUTM)	Period with data
CHS	06L01	Canal	693677	4197269	Oct/00 – Sep/01
CHS	06M01	Benipila	677074	4163725	+

CHS	06P01	Cartagena	673396	4163483	Oct/04 – Sep/12
CHS	06P02	Torre Pacheco	676887	4179896	
CHS	06P03	Perin	667793	4165726	
CHS	06P04	Murta	657453	4188116	
AEMET	AEMET_SJ (*)	San Javier	693425	4184665	Oct/00 – Sep/12
SIAM	CA12	Palma	680675	4173267	Jul/05 – Sep/12
SIAM	CA21 (*)	Corvera	665209	4188766	Oct/00 – Sep/12
SIAM	CA42 (*)	Balsa Pintada	664813	4179533	
SIAM	CA52 (*)	Aljorra	670129	4171693	
SIAM	CA72 (*)	Roche	683620	4166587	
SIAM	TP22 (*)	San Javier	691976	4184939	
SIAM	TP42 (*)	Torre Blanca	685074	4182798	
SIAM	TP52	Mirador	686200	4191066	Abr/09 – Sep/12
SIAM	TP73 (*)	Cayetano	682041	4188284	Oct/00 – Sep/12
SIAM	TP91	Torre Pacheco	677368	4179725	Jul/05 – Sep/12

Stations with (*) were used for building the 'fictitious station'.

During the period with data, the number of total gaps found in the meteorological database was extremely low (Table 4). The missing values in each "target station" were filled using a regression-based approach [*Ramos-Calzado et al.*, 2008]. Simple linear regressions were extracted between monthly series of the "target station" and a "fictitious station" statistically built with the precipitation data of a selected sample of neighbour stations (those ones with a complete dataset – marked with an asterisk in Table 3). When existing, monthly gaps were filled as

$$pre(tg) = a \cdot pre(fict) + b$$

Equation 15

where *pre(tg)* is the estimated precipitation in the target station, *pp(fict)* is the arithmetic average value resulting from rainfall measurements reported in the neighbour stations, and *a* and *b* are the slope and y-intercept resulting from the correlation between both time series (Table 4).

Table 4. Number of gaps filled per station and slope, y-intercept and correlation coefficients between the "target" and "fictitious" stations.

ID Station	No gaps filled	a	b	R^2
06L01	1	0.876	4.50	0.77
06M01	1	0.673	5.80	0.84
06P01	1	0.635	7.01	0.86
06P02	1	0.802	5.42	0.88
06P03	1	0.724	5.67	0.87

06P04	1	0.888	3.74	0.80
AEMET_SJ	0	0.788	4.31	0.84
CA21	1	1.079	2.16	0.84
CA42	0	0.861	4.05	0.88
CA52	1	0.841	3.93	0.89
CA72	0	0.787	2.19	0.89
TP22	0	0.878	3.55	0.86
TP42	1	0.926	1.64	0.92
TP73	0	0.928	3.26	0.91
CA12	3	0.572	6.84	0.84
TP91	0	0.871	4.46	0.90
TP52	0	0.910	3.25	0.94

2.3.1.2 Spatial interpolation

A tension spline interpolation was used to obtain monthly precipitation surfaces. This exact interpolation method results in gentle surfaces (splines) which pass through the inputs points but minimizing the total curvature of the surface. The most gently surface is achieved by minimizing the cumulative sum of squares of the second derivative terms of the surface taken over each control point on the surface. Against the regularized type, the tesion spline type includes the first-derivative into the minimization criteria [*Naoum and Tsanis*, 2003] which results in less smooth surfaces with values more closely constrained by the sample data range. In the tension spline method, two user-defined parameters must be taken: a) the weight of the tension parameter, and b) the number of points used in the calculation of each interpolated cell. The tension parameter specifies the weight attached to the first-derivative terms during minimization: as larger is the tension parameter, less is the stiffness of the plate (a weight of zero results in the basic thin plate spline interpolation). Its value ranges between 0 and 10. For this project a tension value of 5 and a total of 12 points were selected. A map with the mean annual isohyets in the study area is presented in Figure 8.

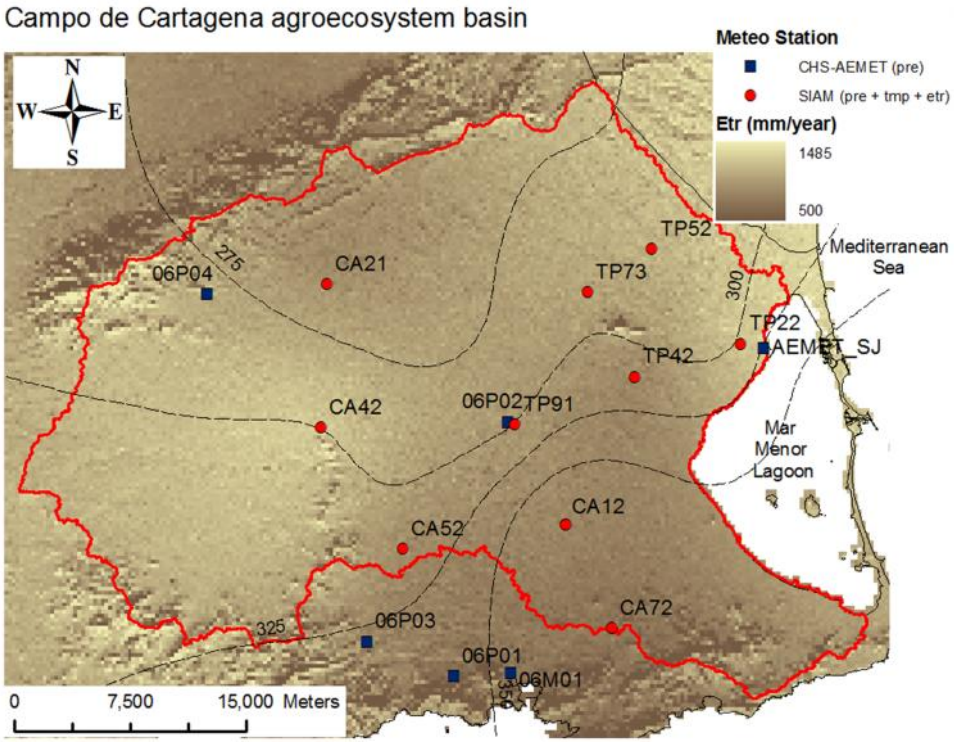

Figure 8. Mean annual precipitation (isohyets) reference evapotranspiration estimated for the Oct2000-Sep2011 period.

2.3.2 Reference evapotranspiration

Spatial fields of monthly *etr* have been estimated according the Hargreaves-Samani equation as,

$$etr = a \cdot rad \cdot (tmp + b) \cdot (tmx - tmn)^{0.5}$$

Equation 16

where *rad* is the incoming solar radiation at the land surface level (MJ month^{-1} m^{-2}); *tmp*, *tmx* and *tmn* are the monthly average values computed from the mean, maximum and minimum daily temperatures, respectively; and *a* and *b* are calibration coefficients estimated for the region using the FAO-Penman-Monteith ET0 ($ET0_{FAO\text{-}PM}$) values measured at different agrometeorological stations located in Campo de Cartagena (SIAM stations in Table 3).

The calibration of Equation 16 was performed station-by-station (Table 5) using radiation estimates from POTRAD5 (see section 2.3.2.2). Because no important spatial variability has been observed in the study region between observed and predicted values of *etr*, one regional-calibrated equation (Figure 9) was finally taken. Additionally, a preliminary assessment of the spatial and seasonal variability of the residuals between observed and predicted values show no significant differences between them (Figure 10).

Table 5. Local calibration of the Hargraves-Samani equation.

ID Station	a parameter			b parameter			R2
	Estimate	LC	UC	Estimate	LC	UC	
CA12	0.0013	0.0011	0.0015	25.4	17.0	33.9	0.96

CA21	0.0007	0.0006	0.0009	71.9	49.3	94.6	0.96
CA42	0.0011	0.0010	0.0012	29.9	24.7	35.1	0.98
CA52	0.0012	0.0010	0.0014	35.6	27.3	43.9	0.97
CA72	0.0015	0.0013	0.0017	21.9	16.5	27.3	0.98
TP22	0.0018	0.0013	0.0023	10.2	1.4	19.1	0.76
TP42	0.0015	0.0014	0.0017	20.0	15.2	24.9	0.96
TP52	0.0015	0.0013	0.0017	22.1	16.6	27.6	0.99
TP73	0.0018	0.0016	0.0020	17.1	13.2	21.0	0.97
TP91	0.0011	0.0009	0.0013	29.0	21.2	36.8	0.97
All stations	**0.0014**	0.0013	0.0015	**25.2**	21.6	28.7	0.89

LC and UC design the 95% lower and upper confidence limits, respectively.

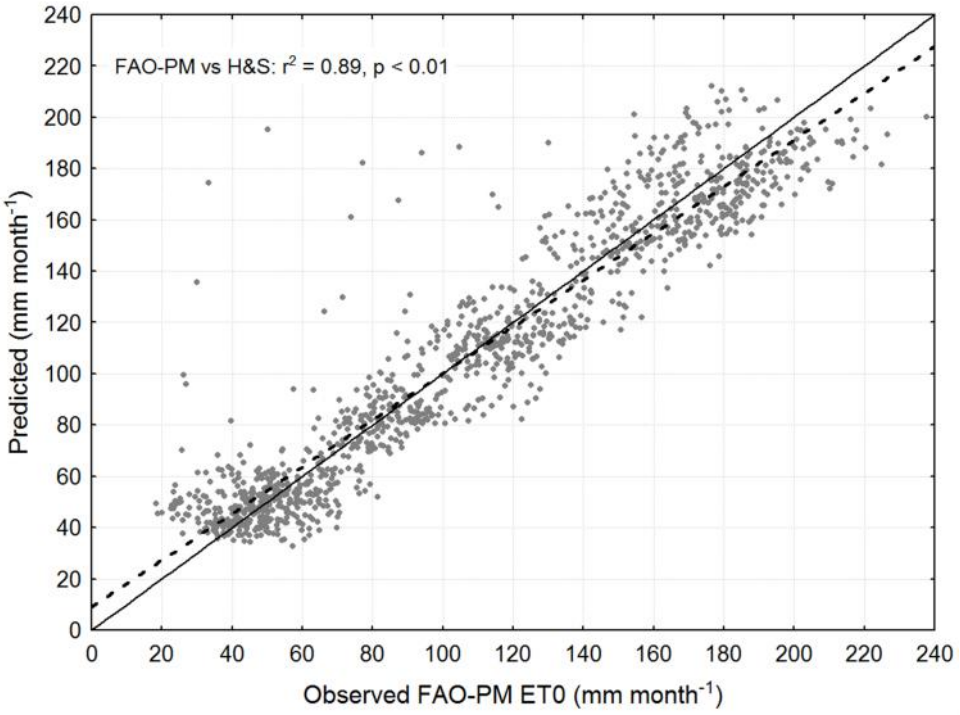

Figure 9. FAO-PM against calibrated Hargreaves-Samani reference evapotranspiration.

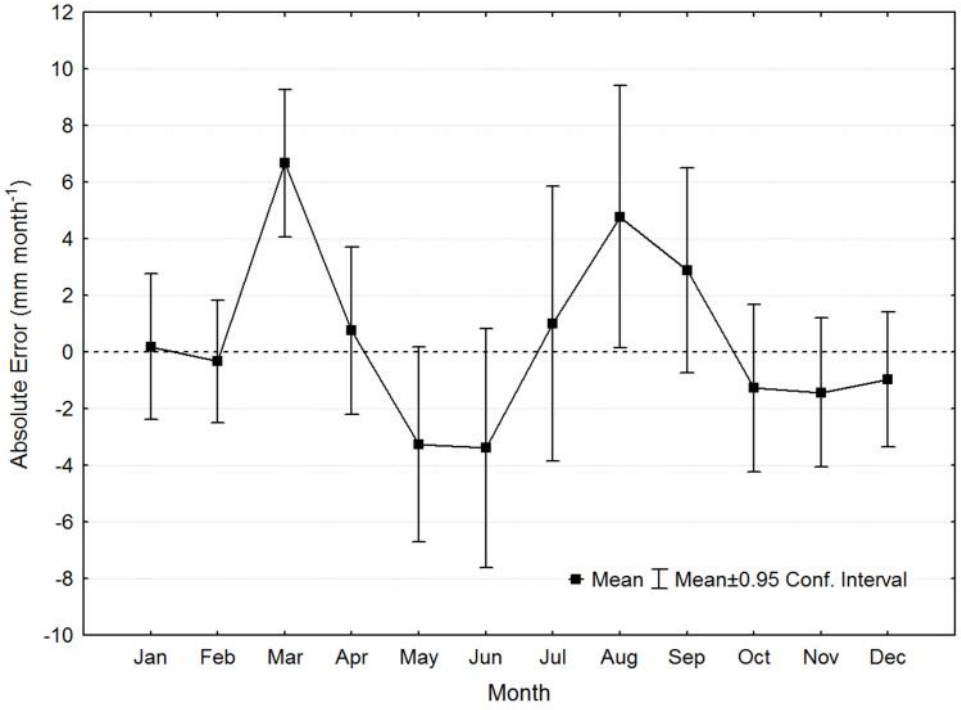

Figure 10. Seasonal dynamics of residuals between FAO-PM and Hargreaves-Samani reference evapotranspiration values at the SIAM stations. Error bars denote the interannual variability.

2.3.2.1 Temperature fields

Similarly to precipitation, monthly spatial fields of *tmx*, *tmn*, and *tmp* required to compute *etr* by Equation 16 were obtained using a tension spline interpolation. Same weight tension parameter (value=5) and number of stations (value=12) were taken.

2.3.2.2 Radiation fields

Maps of incoming solar radiation were computed using POTRAD5 code developed by van Dam [2000]. POTRAD5 has been written in PCRaster language, and it computes both direct and diffuse hourly radiation reaching the surface based on the solar geometry and a digital elevation model. For our purposes, potential values of monthly incoming radiation were estimated assuming no clouds and a transmissivity of the air of 0.6. For calibration of Equation 16, the twelve monthly values of potential incoming surface radiation computed by POTRAD5 along one year were assumed constant during the study period (2000-2012) for all the target stations used in the calibration.

2.3.3 Greenness and crop coefficient dynamics

2.3.3.1 NDVI pre-processing and post-processing

For the WIS-CT, NDVI values from the MOD13Q1 land product of MODIS (tile h17v05) [*Solano et al.*, 2010] was collected covering the period from mid of February 2000 through December 2012. This product consists of16-days MVC (Maximum Value Composite) maps at 250 m of spatial resolution (23 scenes per year). MOD13Q1 product includes a quality layer which reports pixel-by-pixel on the overall pixel reliability and the related specific conditions. According to this MODIS-quality layer, raw MCVs of NDVI were filtered depending on the criteria shown in Table 6.

After excluding pixel values with low reliability, raw NDVI data were filtered using a local polynomial function based on an adaptive Savitzky-Golay filter. Filtering of satellite-based VIs is a critical and widely used practice to remove spike and spurious values, fill non data values, and to extract the downward trend typically observed in the vegetation indices as consequence of atmospheric effects [*Jönsson and Eklundh*, 2002; *Chen et al.*, 2004]. The Savitzky-Golay post-filtering of NDVI fields was done using the TIMESAT software [*Jönsson and Eklundh*, 2004]. A time window of 5 consecutive MCVs, a double iteration to the upper envelope, and an adaptive strength of 2 in a scale from 1-12 was used. Between 85-95% of the catchment was filtered and filled with this post-processing.

Monthly layers of NDVI for twelve hydrological years, from October-2000 to September-2012 were finally computed averaging the composites of each month. From the monthly satellite dataset, a second spatially-based filling procedure was applied for those pixels not effectively filled with TIMESAT. In those cases, the average value resulting from a kernel-window of 7x7 pixels were used, or a constant value of 0.1 was adopted if the kernel filter failed.

Table 6. Quality criteria used to retain (in blue), or not (in red), raw values of NDVI collected from the MOD13Q1 product.

BIT	Long Name	Value	Key
0–1	MODLAND_QA	00	VI produced, good quality
		01	VI produced, but check other QA
		10	Pixel produced, but most probably cloudy
		11	Pixel not produced due to other reasons
2–5	VI usefulness	0000	Highest quality
		0001	Lower quality
		0010	Decreasing quality
		0100	Decreasing quality
		1000	Decreasing quality
		1001	Decreasing quality
		1010	Decreasing quality
		1100	Lowest quality
		1101	Quality so low that it is not useful
		1110	L1B data faulty
		1111	Not useful for any other reason/not
6–7	Aerosol quantity	00	Climatology
		01	Low
		10	Average
		11	High
8	Adjacent cloud detected	1	Yes
		0	No
9	Atmosphere BRDF correction performed	1	Yes
		0	No
10	Mixed Clouds	1	Yes
		0	No
11–13	Land/Water Flag	000	Shallow ocean
		001	Land (Nothing else but land)
		010	Ocean coastlines and lake shorelines
		011	Shallow inland water
		100	Ephemeral water
		101	Deep inland water
		110	Moderate or continental ocean
		111	Deep ocean
14	Possible snow/ice	1	Yes
		0	No
15	Possible shadow	1	Yes
		0	No

2.3.3.2 Greenness dynamics

To evaluate the seasonal greenness trajectories of the main land use cover type in the region, NDVI values were extracted from three locations with different cultivars. As it can be checked in Figure 11, irrigated Citrus orchards show the highest greenness values in the region, with maximum values reached during the late autumn and early winter. The inter-annual average NDVI trajectory in the plot with row crops shows a higher seasonality (range between the maximum and minimum NDVI) than in the Citrus case. In plots dominated by row crops, NDVI values remain relatively high from November to April with two relative maxima in December and end of March matching with peak values for winter and spring-summer row crops (Figure 12, Figure 13). Against the irrigated cultivars (Citrus and row crops), rainfed orchard trees (olive and almond trees) show the lowest average and range values of NDVI.

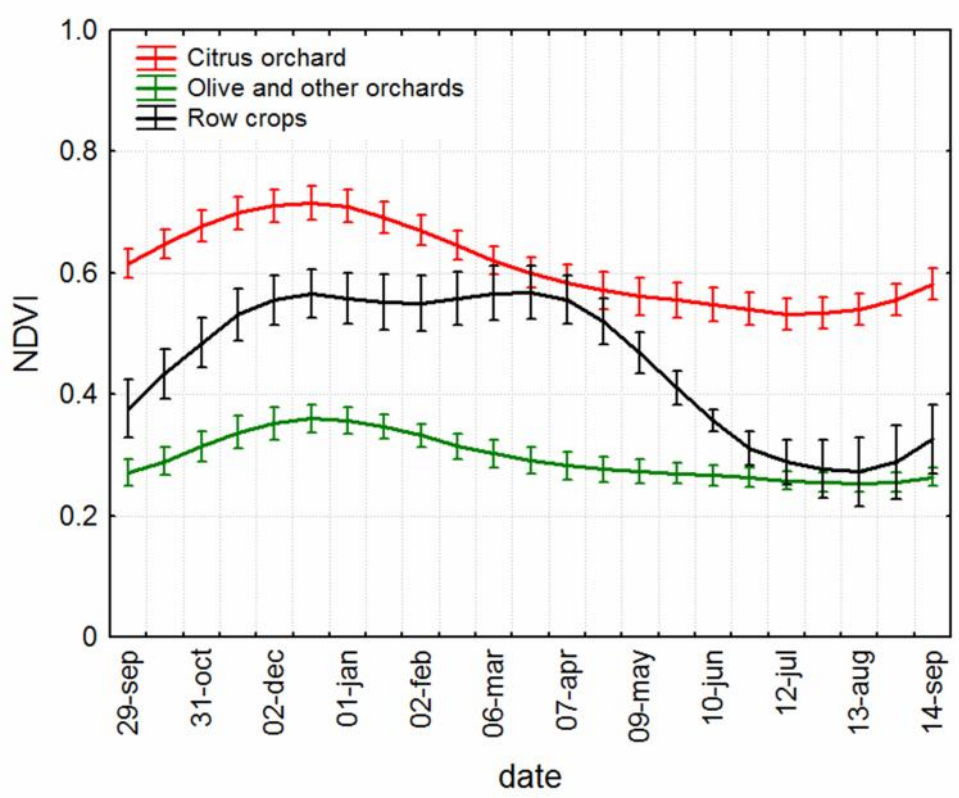

Figure 11. Average NDVI trajectories (Oct2000-Sep2012) at three cultivars with irrigated Citrus trees, rainfed trees (olive and almonds) and horticulture-row crops. Bars denotes ±95% confidence intervals for the inter-annual variability.

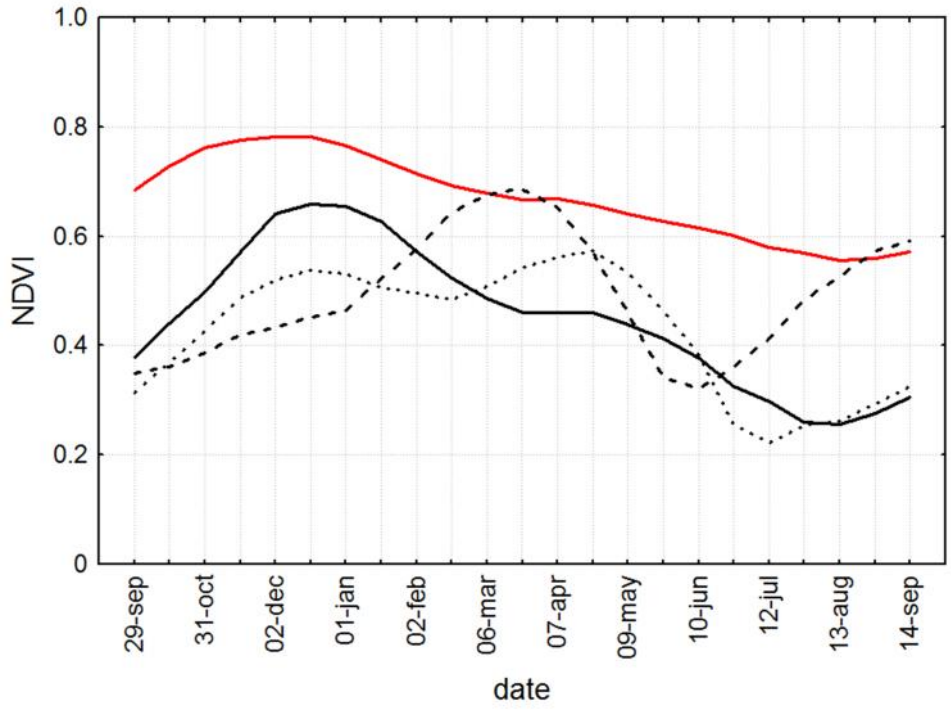

Figure 12. Annual NDVI trajectories observed at a site with a Citrus orchard (red), a winter row crop (solid black), a spring row crop (dashed black), and a two crop rotation cycle (dotted black).

Seasonal-averaged spatial fields of NDVI are finally shown in Figure 13. As can be seen, vegetation density is highest within the black polygons that correspond to the Campo de Cartagena irrigation district. Also outside of this district some areas are irrigated, and show high NDVI values. Maximum productivity is during winter and autumn.

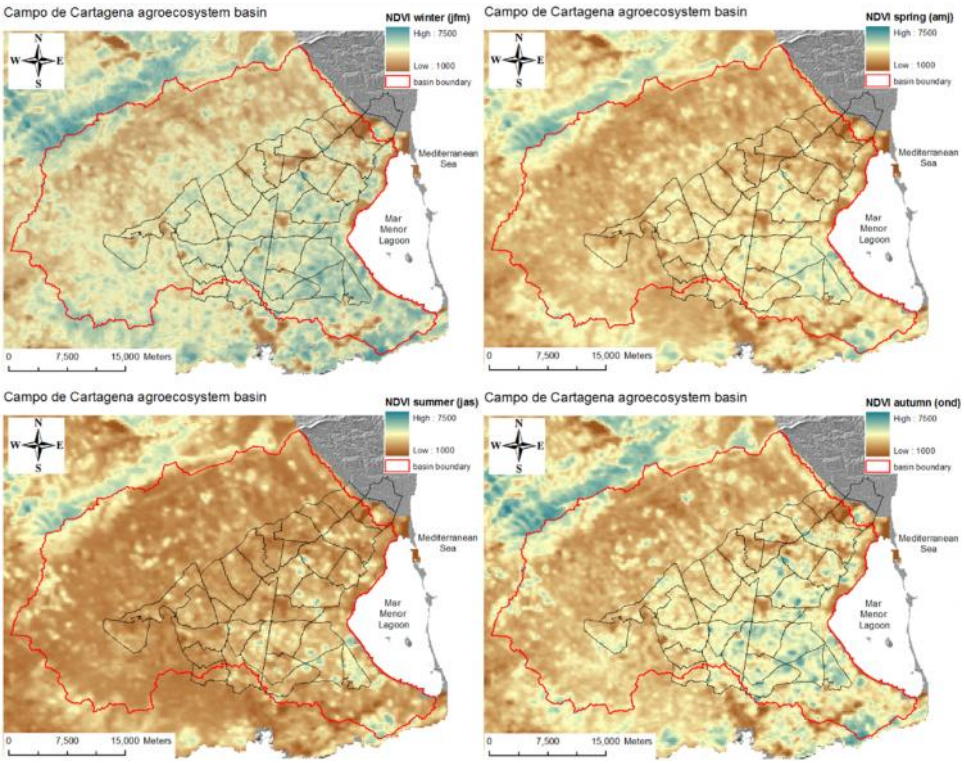

Figure 13. Maps of seasonally-averaged NDVI in the Campo de Cartagena basin. NDVI values are scaled by *10000, and scale legend in the 1000-7500 range.

2.3.3.3 Crop coefficient parameterization

The parameterization of the NDVI-k_c function is critical in SPHY to estimate actual evapotranspiration. The good performance in adopting a linear relationship model between NDVI and k_c has been highlighted by several studies [*Singh and Irmak*, 2009; *Kamble et al.*, 2013; *Mutiibwa and Irmak*, 2013]. However crop specific models have been widely shown to perform better than linear models as they implicitly recognize the functional differences among vegetation groups (e.g. grass *vs* shrubs or tress, or pastures *vs* horticulture crops or tree orchards) [*Glenn et al.*, 2011]. The adoption of a universal-single parameterization has been suggested in large spatial domains in which land use data is not readily available.

In this study, a single-crop and a dual-crop approach have been adopted for the NDVI-k_c parameterization in those areas under irrigation. In the non-irrigated area, it has been assumed the dominance of an open grass-shrub vegetation community with shrubs not taller than 1 m, and in which maximum NDVI and k_c values have been chosen at 0.65 [*Descheemaeker et al.*, 2011]. Against the single crop-approach, the dual-crop approach recognizes a crop-specific NDVI-kc relationship which takes into account the dominance at the pixel level of *Citrus* orchards against row-vegetable crops. Table 7 shows the values adopted for the NDVI-k_c parameters in both approaches, and the linear relationships derived when the observed NDVI ranges between the maximum and minimum NDVI thresholds. The NDVI-k_c functions are graphically shown in Figure 14 (single-crop approach) and Figure 15 (dual-crop approach).

In order to perform the dual-crop approach in the irrigated area, the land use cover map supplied by the SIOSE2005 project was used (Figure 2) (for a detailed description of the SIOSE project see http://www.siose.es). This project provides an object-oriented land cover model from which pure polygons (100% covered) of citrus orchards and herbaceous-row crops could be identified. In this study, the *Citrus*-based NDVI-k_c parameterization was also adopted for those polygons classified as "mosaic of land cover types" but with a percentage of *Citrus* coverage higher than 50%. If not, the row crop-dominated parameterization is finally taken.

Representative figures for the maximum NDVI thresholds expected for *Citrus*-dominated and row crops-dominated pixels were extracted from the annual NDVI trajectories observed in a sample of "pure" pixels located in the study area. Maximum value of k_c for *Citrus*-dominated pixels was calibrated from actual measurements of evapotranspiration in *Citrus* experimental fields (see section 2.4), while maximum k_c value for row-dominated pixels was averagely fitted according to the maximum values of basal k_c reported in the region for these crops by [*Villalobos et al.*, 2006].

Table 7. NDVI-kc parameterization used in WIS-CT.

Land cover Types	**Non-irrigated area** (native vegetation)	**Irrigated area**		
		Single-crop approach	Dual-crop approach	
			Citrus-dominated	Row crop-dominated
[$NDVI_{min}$ / $k_{c,min}$]	0.10 / 0.05	0.10 / 0.05	0.10 / 0.05	0.10 / 0.05
[$NDVI_{max}$ / $k_{c,max}$]	0.65 / 0.65	0.70 / 0.80	0.65 / 0.68	0.85 / 1.00
Values of kc for NDVI between				
[-1, $NDVI_{min}$]	0.05	0.05	0.05	0.05
($NDVI_{min}$, $NDVI_{max}$]	-0.0591+1.091·*x*	-0.0750+1.250·*x*	-0.0645+1.145·*x*	-0.0767+1.457·*x*
($NDVI_{max}$, 1]	0.65	0.80	0.68	1.00
Kamble's function	-0.1725+1.457·*x*	[*Kamble et al.*, 2013]		
Mutiibwa's function	-0.1100+1.580·*x*	[*Mutiibwa and Irmak*, 2013]		

x = NDVI

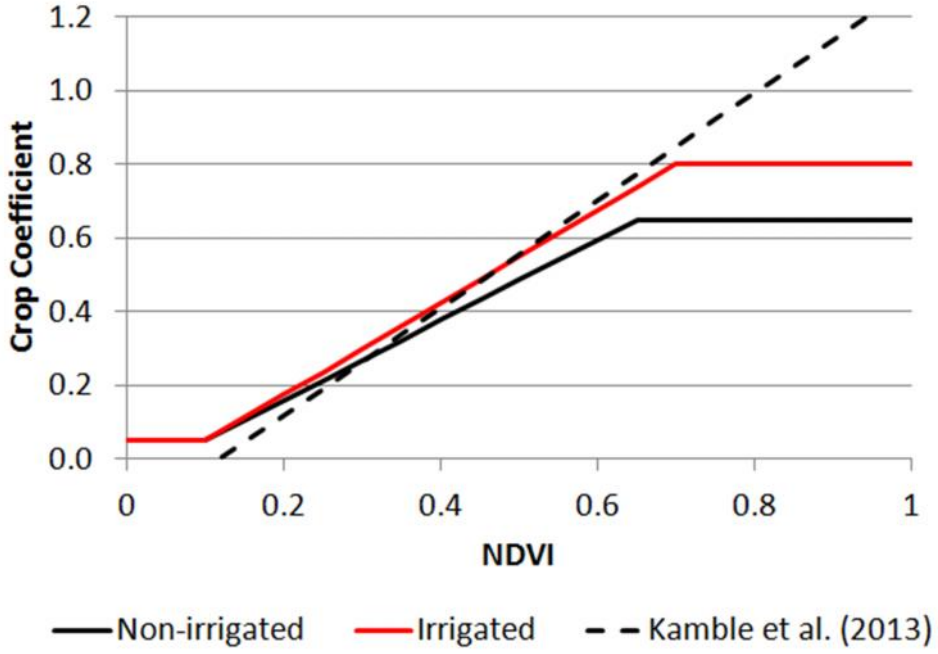

Figure 14. Relationship between NDVI and k_c for irrigated and non-irrigated areas (single-crop based approach).

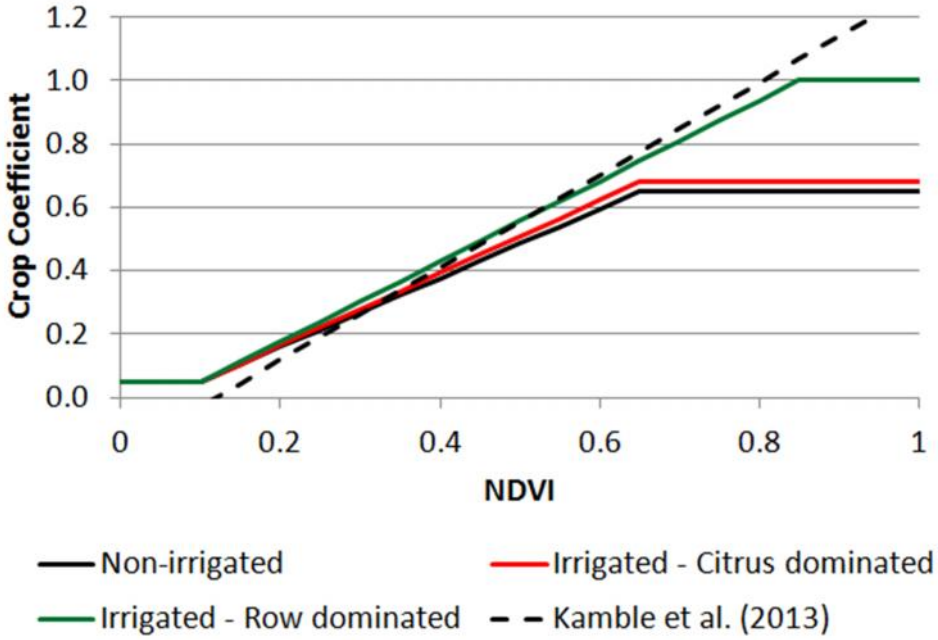

Figure 15. Relationship between NDVI and k_c for irrigated and non-irrigated areas (dual-crop based approach).

2.3.4 Soil and soil hydraulic parameters

Maps of texture (percentage of sand, silt and clay), organic matter and gravimetric water content at 15 (wilting point) and 3 atm (field capacity) in the topsoil layer (from the surface up to 30-40 cm in depth) were supplied by the Soil and Water Conservation Research Group at CEBAS-CSIC [*Pérez-Cutillas*, 2013]. Spatial layers were elaborated at the regional level (province of Murcia) from pedotransfer functions in which landscape attributes, extracted from

satellite-based data and a DEM layer, were correlated at different scales against field data collected from the Spanish National Soil Database and the LUCDEME project.

Before to be used in SPHY, spatial layers of gravimetric water contents had to be converted in volumetric units using bulk density estimates as

$$pF(\%vol) = \frac{pF(\%grav)}{BD}$$

Equation 17

where *BD* is the bulk density (g/cm^3) estimated from textural data according the empirical relationships developed by [*Hollis et al.*, 2012], as

$$BD_{cult} = 0.80806 + 0.823844 \cdot \exp(-0.27993 \cdot OC) + 0.0014065 \cdot sand - 0.0010299 \cdot clay$$

Equation 18

$$BD_{\min} = 0.69794 + 0.750636 \cdot \exp(-0.230355 \cdot OC) + 0.0008687 \cdot sand - 0.0005164 \cdot clay$$

Equation 19

in which *OC* is the soil organic carbon in % (a conversion factor of 1.72 between OC and MO was assumed), and *sand* and *clay* are the % of these soil fractions in the topsoil. *BD* values were estimated depending if the topsoil is cultivated (*cult*) or not (*min* refers to all other mineral horizons).

Finally, lookup-table values for saturated hydraulic conductivity -K_{sat}- and effective porosity -n_e- were adopted from [*Fernandez-Illescas et al.*, 2001] according to the textural soil classes retrieved in the area from the layers supplied by Cutillas' dataset (Table 8, Figure 16).

Table 8. Average values of effective porosity (%) and saturated hydraulic conductivity (cm/h) according the main USDA soil textural classes in the region.

ID Class	Text_Class[1]	n_e[2]	log K_{sat}[3]
2	Loamy sand	38.6	-0.152
3	Sandy loam	41.6	-0.520
4	Loam	43.5	-0.749
7	Clay loam	44.9	-0.917
8	Sandy clay loam	41.6	-0.520
12	Clay	46.1	-1.070

1 Textural class according to USDA soil code
2 Effective porosity in % (from Fernandez-Illescas et al., 2001)
3 Saturated hydraulic conductivity in cm/h (from Fernandez-Illescas et al., 2001)

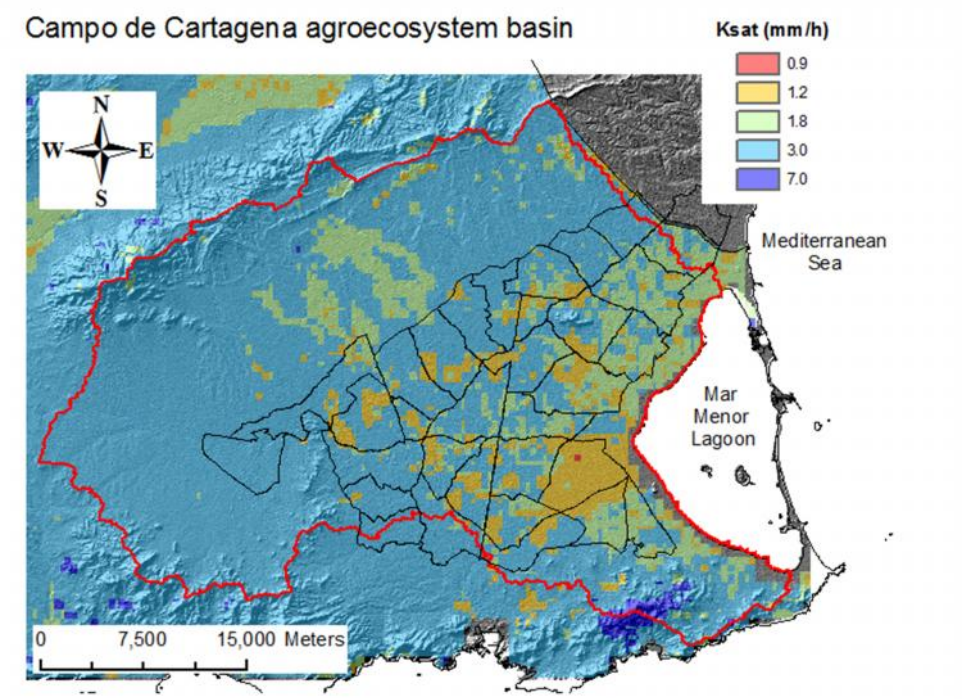

Figure 16. Saturated hydraulic conductivity values for the soil textural classes retrieved in the region.

As stated previously, soil depth is a critical parameter in SPHY because it regulates the capacity of the soil to store water, to generate surface runoff by saturation and to provide water to vegetation. For this study, a soil depth layer (was computed using a simple slope-dependent function, as

$$Z = Z_{\max} \cdot (100 - slope)$$

Equation 20

where Z_{max} is considered here as the representative soil depth typically found in the flattest landscape areas, and *slope* is the local slope, in percentage, computed from the local DEM. This approach does not take into account the topographic position of each pixel in the landscape. Future improvements in SPHY will include the estimation of soil depth from a topographic index which combines information on steepness and specific catchment area.

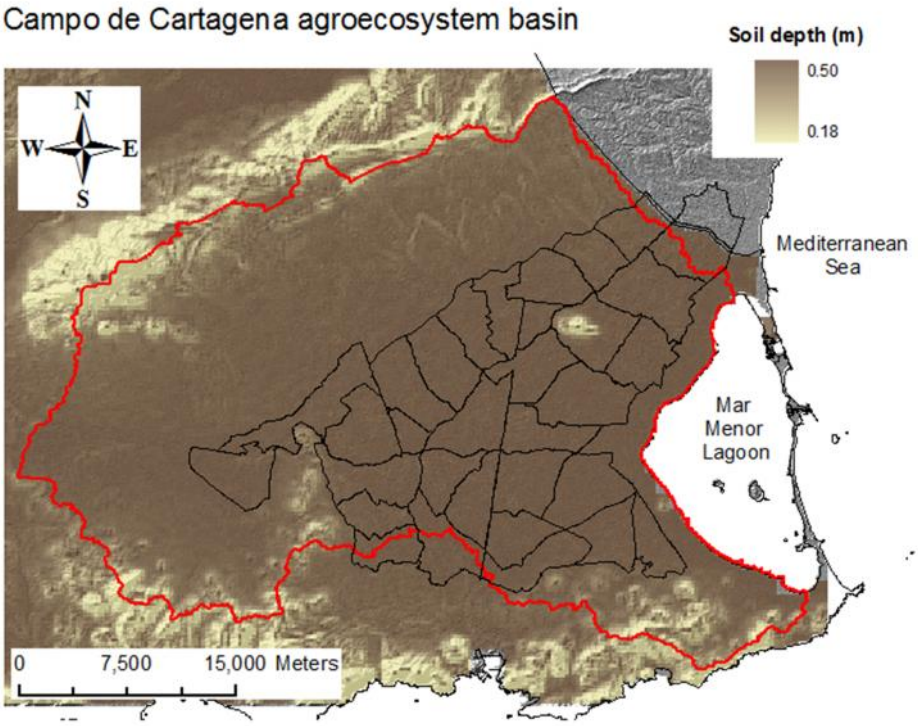

Figure 17. Soil depth layer in WIS-CT.

2.4 Calibration and validation sites

A dataset of daily actual evapotranspiration measurements at two sites (Villa Antonia -VA- y Casa Mulero -CM-, Figure 18) in the irrigated area was available for calibrating and evaluating the CC-VI approach. Both ECSs and their respective databases are being managed by the Agroforestry Department of the Polytechnic University of Cartagena. In both experimental sites, actual ET measurements were collected by an Eddy Covariance System (ECS) every 30 min. and post-filtered using standardized protocols. Data for VA used in this study was available from July-2009 to September-2012, while for CM from July-2009 to August-2011 (Figure 19). Both ECSs were installed in plots strongly dominated by *Citrus* orchards. Canopy cover in VA is 80% against 50% in CM. Although tree density is lower in VA than in CM (417 *vs* 741), VA is characterized by a more stabilized and mature orchard system than CM [*SIRRIMED*, 2012]. As consequence, VA system is characterized by its higher annual-average NDVI values and lower intra-annual seasonality greenness dynamics (Figure 20). Here, actual data from both ECS were used for: a) firstly, verifying the robustness of the k_c-NDVI approach in estimating actual evapotranspiration, and the implicit assumption regarding the existence of a linear relationship between both variables, and b) secondly, calibrating the k_c-NDVI relationship for *Citrus*-dominated pixels. To accomplish both purposes, daily data from the ECS database were aggregated at 16-days and monthly scales, and actual k_c were computed as the ratio between actual and reference evapotranspiration rates at each time window.

Figure 18. Location of validation sites. MODIS 250 m. grid-mesh is superimposed over the ortophoto.

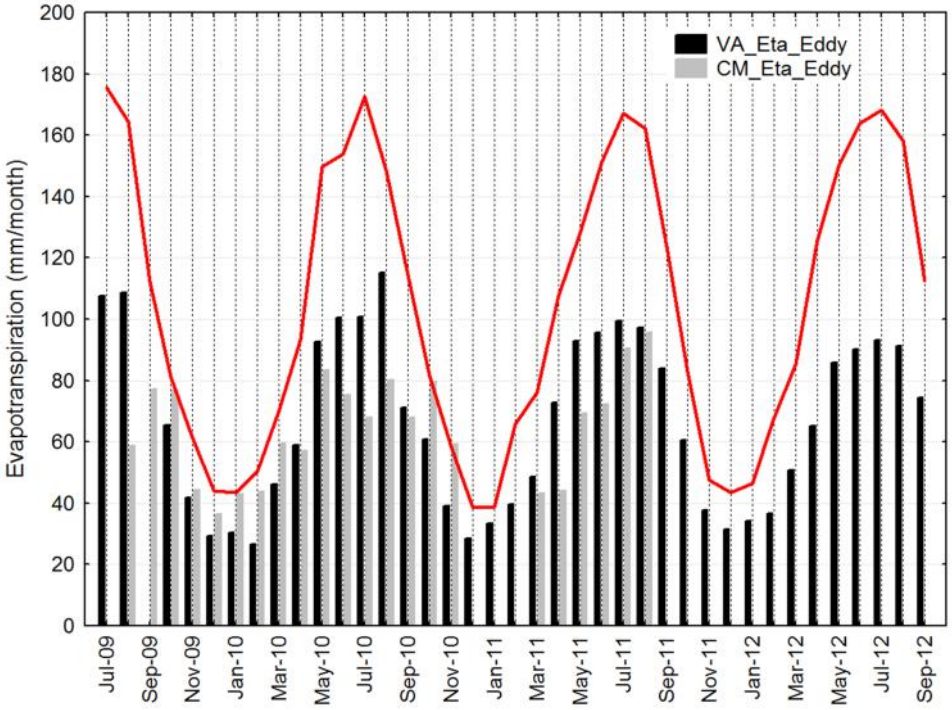

Figure 19. Monthly rates of actual evapotranspiration in Villa Antonia (VA) and Casa Mulero (CM) experimental sites, and reference evapotranspiration (red) at the closest SIAM-agrometeorological station.

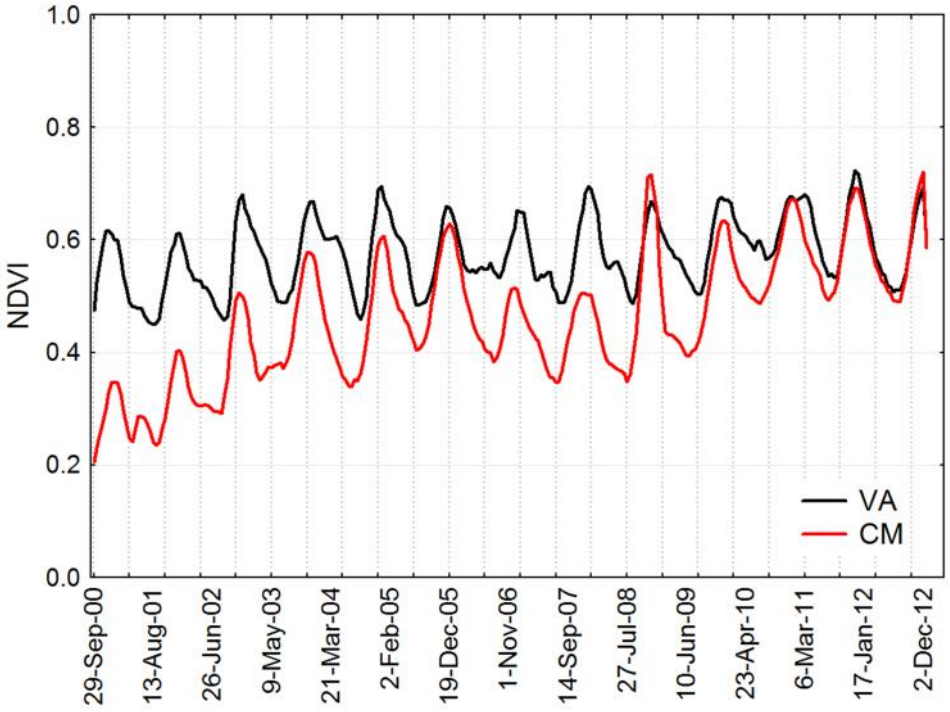

Figure 20. Greenness dynamics observed in VA and CM experimental sites.

The overall performance of the CC-VI approach for estimating evapotranspiration was evaluated at the Villa Antonia experimental site using different simple statistics (Mean Absolute Error -MAE- and Root Mean Square Error -RMSE-) and other efficiency indicators (coefficient of determination -R^2-, Nash-Sutcliffe efficiency -E-) (see equations below). The Nash-Sutcliffe efficiency is widely used as an indicator of the temporal correlation between two variables [*Legates and McCabe Jr.*, 1999; *Krause et al.*, 2005]. The range of E lies between 1.0 (perfect fit) and -∞. An efficiency of lower than zero indicates that the mean value of the observed time series would have been a better predictor than the model. These measures were computed at the year and month scale to test the goodness of the single and dual-crop based NDVI-k_c parameterizations, and to calibrate the NDVI-k_c function for pixels dominated by *Citrus* orchards.

$$MAE = \frac{\sum_{i=1}^{n} |P_i - O_i|}{n}$$

Equation 21

$$RMSE = \frac{\sum_{i=1}^{n} (P_i - O_i)^2}{n}$$

Equation 22

$$R^2 = \frac{\sum_{i=1}^{n} (O_i - \overline{O}) \cdot (P_i - \overline{P})}{\sqrt{\sum_{i=1}^{n} (O_i - \overline{O})^2} \sqrt{\sum_{i=1}^{n} (P_i - \overline{P})^2}}$$

Equation 23

$$E = 1 - \frac{\sum_{i=1}^{n} (O_i - P_i)^2}{\sum_{i=1}^{n} (O_i - \overline{O})^2}$$

2.5 Sensitivity analysis

Similarly to Contreras et al. [2008], a sensitivity analysis was performed to assess the effects of variation in parameter inputs on: i) total evapotranspiration met with water from the soil bucket -eta^{sm}-, and ii) total drainage (sum of deep percolation and surface runoff). Following Finch [1998] , the effect of changing a soil-vegetation input parameter at a time on a variable output was compared against a baseline value resulting for a 'reference boundary domain'. In a first step, the sensitivity analysis was performed at the Villa Antonia experimental site using the SPHY model calibrated for *Citrus*-dominated orchards (see Table 7), and the time series of precipitation and reference evapotranspiration interpolated for the site from October-2000 to September-2012. At this step, sensitivity analysis let us to rank which parameters deserve more attention when model structure uncertainties at the catchment scale are assessed. Sensitivity to a given parameter is evaluated by: 1) plotting the relative changes in an input parameter against the relative changes generated over an objective variable function, and 2) estimating the percentage of change required in an input parameter to yield a 1% and 5% of variation over the objective variable. Although a one-at-a-time design does not allow assessment of the distribution of possible output values, due to interactions among the parameters involved, this approach was preferred over the more complex and computationally more demanding global sensitivity analyses based on random sampling methods (e.g. Monte-Carlo simulations). The model parameters, their reference values and the value ranges tested in the sensitivity analysis are listed in Table 9.

In a second step, the most influential input parameters at Villa Antonia site were chosen to be changed for those values which generated 1% and 5% of change in the selected output variables. Results in evapotranspiration and total drainage at the catchment scale are finally evaluated in an attempt to obtain a preliminary assessment of the model structure uncertainty.

Table 9. Range of values of input parameters, and sensitivity results of SPHY at Villa Antonia experimental site.

	Min	Max	Ref. value	eta^{sm}		dra = roff + per	
				± 1 %	± 5 %	± 1 %	± 5 %
Soil parameters							
Depth	0.15	2.5	0.5	+3.8 (+)	+21.4 (+)	-1.4 (+)	-8.2 (+)
β	12.5	25.0	25.0	-5.6 (-)	-28.7 (+3.0%)	-1.8 (+)	-13.6 (+)
Vegetation-crop parameters							
γ	0.75	2.50	1.0	+42 (-)	+150 (-3.2%)	+29.5 (-)	+150 (-3.9%)
$NDVI_{max}$	0.50	0.80	0.65	-3.8 (+)	-23.1 (+2.6%)	+4.6 (+)	-23.1 (+4.0%) +13.5 (+4.0%)
K_{cmax}	0.55	0.80	0.68	+2.6 (+)	-4.4 (+)	+14.7 (+)	-19.3 (+)

Reference values for: A) Soil parameters: por = 0.416; fc = 0.162; wp = 0.077; log K_{sat} = -0.520; Irrigation loss coefficient = 0.10; B) Vegetation parameters: $NDVI_{min}$ = 0.10; $K_{c,min}$ = 0.05; Interception coefficient = 0.05.
Initial soil moisture at the beginning of the simulation = 0.10.

2.6 Water accounting, and estimation of groundwater pumping rates from ancillary data

Water accounting diagrams have been built for the Campo de Cartagena basin based on the meteorological and model outputs retrieved from SPHY. In addition to the main water balance components in both irrigated and non-irrigated areas, data on the volume of water delivered to the irrigated farmland from the Tajo-Segura aqueduct was used. At the basin scale, total water pumped from aquifers is computed using a balance approach, as

$$swt - cl + gwp = sl + irr$$

Equation 25

where, *swt* = surface water transfer delivered into the system by the Tajo-Segura aqueduct, *cl* = conveyance losses accounted during the distribution of surface water through the first-order channel, *gwp* = volume of water pumped from aquifers and left in the on-site farm water reservoirs, *sl* = storage losses of water accounted in the on-site farm reservoirs, and irr = irrigation inputs estimated for meeting the crop water requirements (computed by SPHY according section 2.2.3).

Data on monthly deliveries of water from the Tajo-Segura aqueduct for the study period have been supplied by the Segura Basin Water Authority (CHS) and the Irrigation Community of Campo de Cartagena (ICCC). Data provided by CHS refer to the gross volume of water entering into the irrigation system, while data from the ICCC refers to the volume of water effectively delivered to the irrigated farmland once conveyance losses have been subtracted.

An average conveyance efficiency rate of 93% was observed and used for estimating the conveyance losses accounted in the first-order distribution system. As an usual practice in the region, the volume of water resulting after discounting the conveyance losses, plus the groundwater resources pumped from aquifers, are stored in on-site farm open reservoirs just before to be applied at the field scale. In this study, a constant monthly distribution of storage losses in the open reservoirs have been assumed according Martínez-Álvarez et al. [2008].

In this study we assume two main sources of water to meet the irrigation requirements of crops: a) the Tajo-Segura aqueduct, and b) aquifers. However other alternative sources are being actually exploited in the region, i.e. reclaimed and desalinized waters. Because the relative

contribution of these alternative sources is weak in comparison with the deliveries of surface water from the aqueduct and the total volume of water abstracted from aquifers, it is assumed to consider them as a negligible term in the water balance equation (Equation 25).

2.7 Climate change scenarios

The impact of global warming on the water requirements of crops and on the water balance of the Campo de Cartagena basin has been evaluated forcing SPHY with a climate scenario defined by changes in the reference evapotranspiration. To test this, a new set of reference evapotranspiration maps were built using the patterns of change simulated for temperature and incoming solar radiation by the PROMES-UCM Regional Climate Model [*Sánchez et al.*, 2004].

In a recent study performed by the Spanish National Meterological Agency (AEMET) [*Brunet et al.*, 2009], future climate projections derived from different downscaling techniques and Regional Climate Models have been integrated under a common Spanish-national mesh-domain of 112 x 96 pixels with a spatial resolution of 0.44 degress (~50 km) (Figure 21). This database has been elaborated in the framework of the PRUDENCE-ENSEMBLE EU projects, and it can be freely downloaded from the AEMET webpage. Under the PRUDENCE project, the PROMES-UCM Regional Climate Model was nested with the forcing inputs provided by the *HadAM3* Global Climate Model for the A2 and B2 climate scenarios [*IPCC*, 2000]. From the resampled AEMET-PRUDENCE database we extracted the daily values of mean, maximum and minimum temperature, and incoming solar radiation from the closest “land” pixel (target pixel in Figure 21) to our study area. Data was collected for two time periods: i) the reference period, with data from 1961 to 1990, and ii) the future A2 and B2 scenarios with simulated data from 2071-2100.

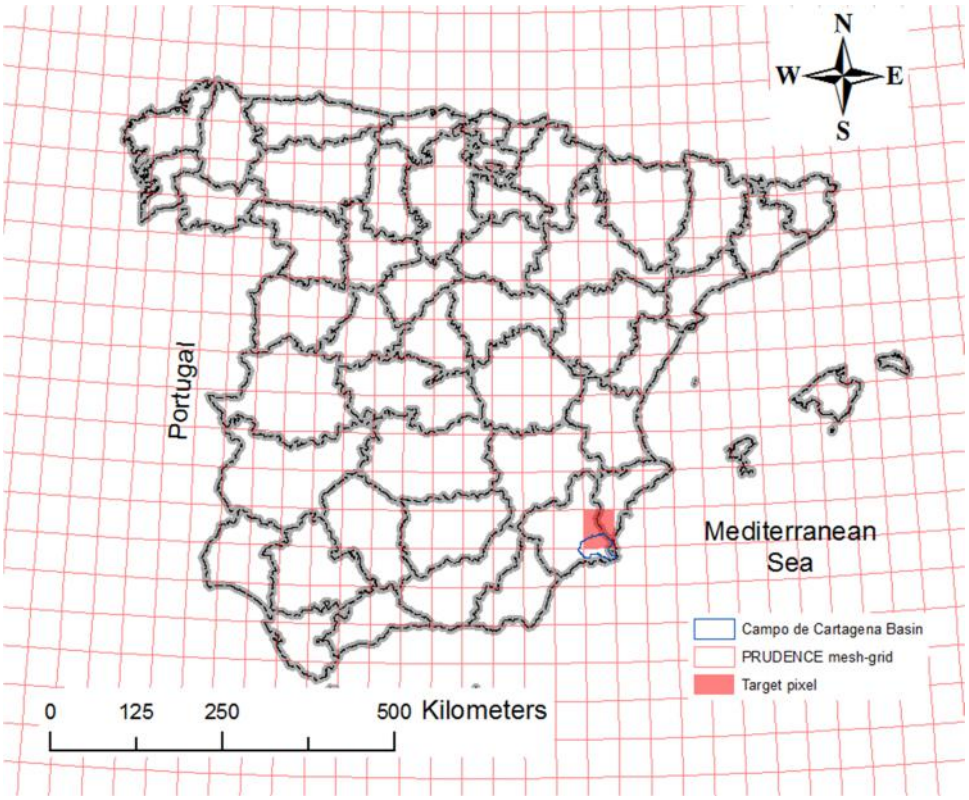

Figure 21. Spanish mesh grid domain used in the framework of the PRUDENCE EU project.

The A2 scenario describes a very heterogeneous world in which local identities are well isolated being the economic development regionally oriented. This scenario assumes a per capita economic growth and a technological change more fragmented and slower than in other defined scenarios. Contrary to the A2 scenario, the B2 scenario describes a world in which local solutions are adopted to reach the economic, social and environmental sustainability. It assumes a continuous growth of population and an intermediate economic development. It is a future scenario oriented towards the environmental protection at the local and regional level.

From the daily database, average monthly trajectories for temperature variables and incoming solar radiation were computed for the reference period and future scenarios. From these data, absolute changes for the temperature variables between periods (Figure 22A-C), and the ratio changes for the shortwave incoming radiation (Figure 22D) are then computed, and finally added to the monthly time serie of temperature and potential surface radiation layers considered in our study. The new time series are then put into together in order to get reference evapotranspiration maps according the Hargreaves and Samani equation described in Equation 16.

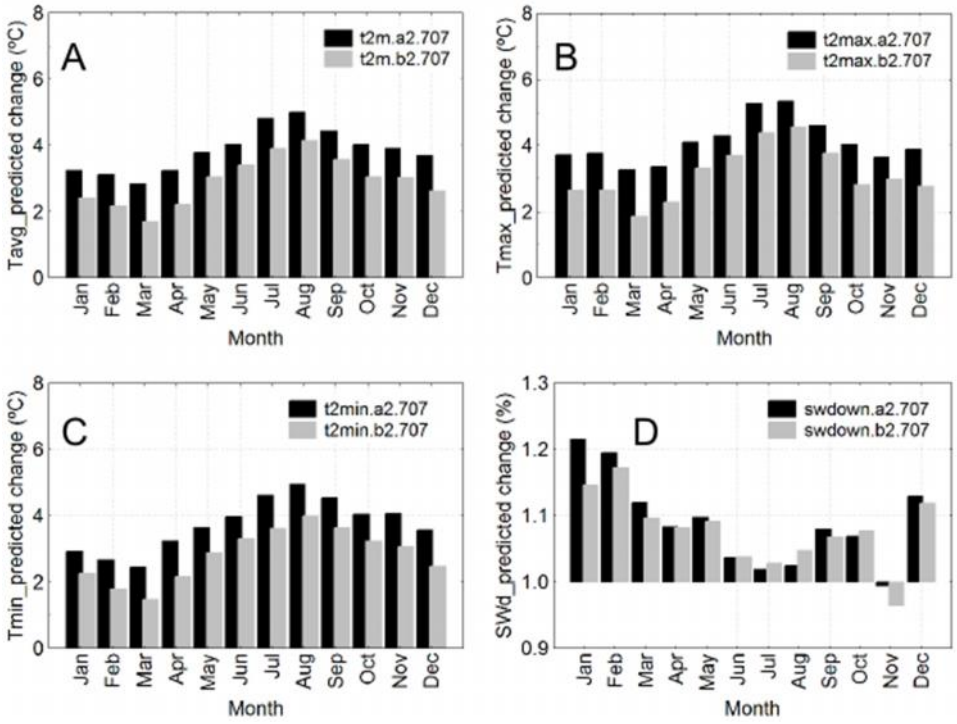

Figure 22. Seasonal predicted changes for tavg (A), tmax (B), tmin (C) and total incoming shortwave radiation (D) between the 1960-1990 reference period and the 2070-2100 A2 and B2 scenarios.

3.1 Performance assessment and calibration of SPHY at a *Citrus*-dominated orchard

The goodness-of-fit measures for the Villa Antonia experimental site (Table 10) indicate a good correspondence between the evapotranspiration estimates derived with the VI-CC approach and the actual Eddy measurements. At the same time, a relatively high variability is observed in the NDVI-k_c scatterplots (Figure 23) measured at both experimental sites. In both sites, and during the calibration period, NDVI values were always higher than 0.40. Despite of the high scatter, the linear relationship between NDVI and k_c was statistically significant ($p<0.01$) and with a coefficient of correlation of 0.22 at both time (16-day and month) scales.

According to the actual data, the time correlations between the actual measurements and the uncalibrated SPHY-based and Kamble-based estimates of monthly evapotranspiration values were extremely high with Nash-Shutcliffe coefficients higher than 0.8. However and despite the high time correlation shown by the NS coefficient, the use of either the Kamble's NDVI-k_c function or the uncalibrated NDVI-k_c parameterization overestimated the actual evapotranspiration observed at Villa Antonia site, advising for the adoption of a crop-specific NDVI-k_c parameterization better adapted to *Citrus*–dominated orchards. Best results for the goodness-of-fit measures were reached at Villa Antonia when a $k_{c,max} = 0.68$ is adopted (Table 10).

At the Casa Mulero experimental site, correspondence between observed and estimated evapotranspiration values was poor (Nash-Sutcliffe efficiency < 0) (Figure 24, Table 11). This may be due to the important role advective processes play in controlling total evapotranspiration at CM, being a much more heterogeneous site than Villa Antonia with a higher surface roughness.

Table 10. Basic statistics and measures of goodness-of-fit for Villa Antonia experimental site.

Villa Antonia	Actual	SPHY (uncalibrated)	SPHY (calibrated)	SPHY (Kamble)
Eta 2009-2010	761	835	767	870
Eta 2010-2011	788	857	782	891
Eta 2011-2012	752	857	782	886
Annual Average	767	850	777	882
MAE (mm year^{-1})		82.4	13.9	115.3
RMSE (mm year^{-1})		83.9 (11%)	17.9 (2%)	116.1 (15%)
MAE (mm month^{-1})		8.1	5.0	10.2
RMSE (mm month^{-1})		9.8 (15%)	7.0 (11%)	11.9 (18%)
R^2 (Actual vs Predicted)		0.93	0.93	0.93
N-S Efficiency (n=38)		0.87	0.93	0.81

Table 11. Basic statistics and measures of goodness-of-fit for Casa Mulero experimental site.

Casa Mulero	Actual	SPHY (uncalibrated)	SPHY (calibrated)	SPHY (Kamble)
Eta 2009-2010	719	717	662	733

MAE (mm month^{-1})	15	14	15
RMSE (mm month^{-1})	18 (30%)	17 (27%)	19 (30%)
R^2 (Actual vs Predicted)	0.40	0.40	0.40
N-S Efficiency (n=22)	-0.26	-0.07	-0.31

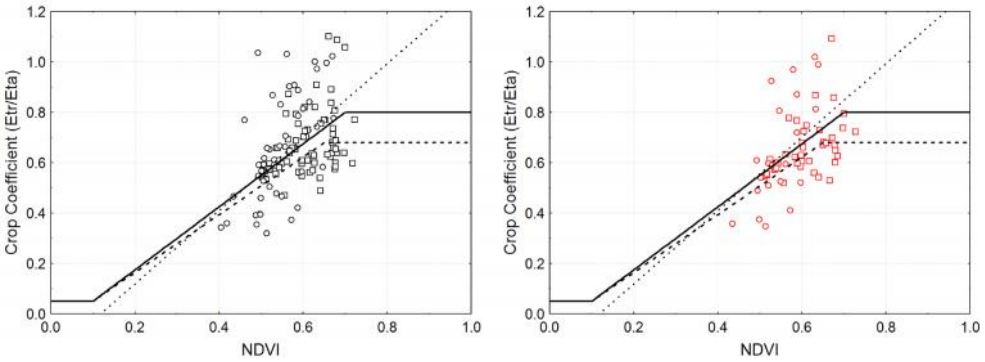

Figure 23. Actual NDVI-k_c scatterplots for VA (squares) and CM (circles) computed at 16-days (left panel) and monthly (right panel) scales. Uncalibrated (solid), *Citrus*-calibrated (dashed) and Kamble's (dotted) functions are shown.

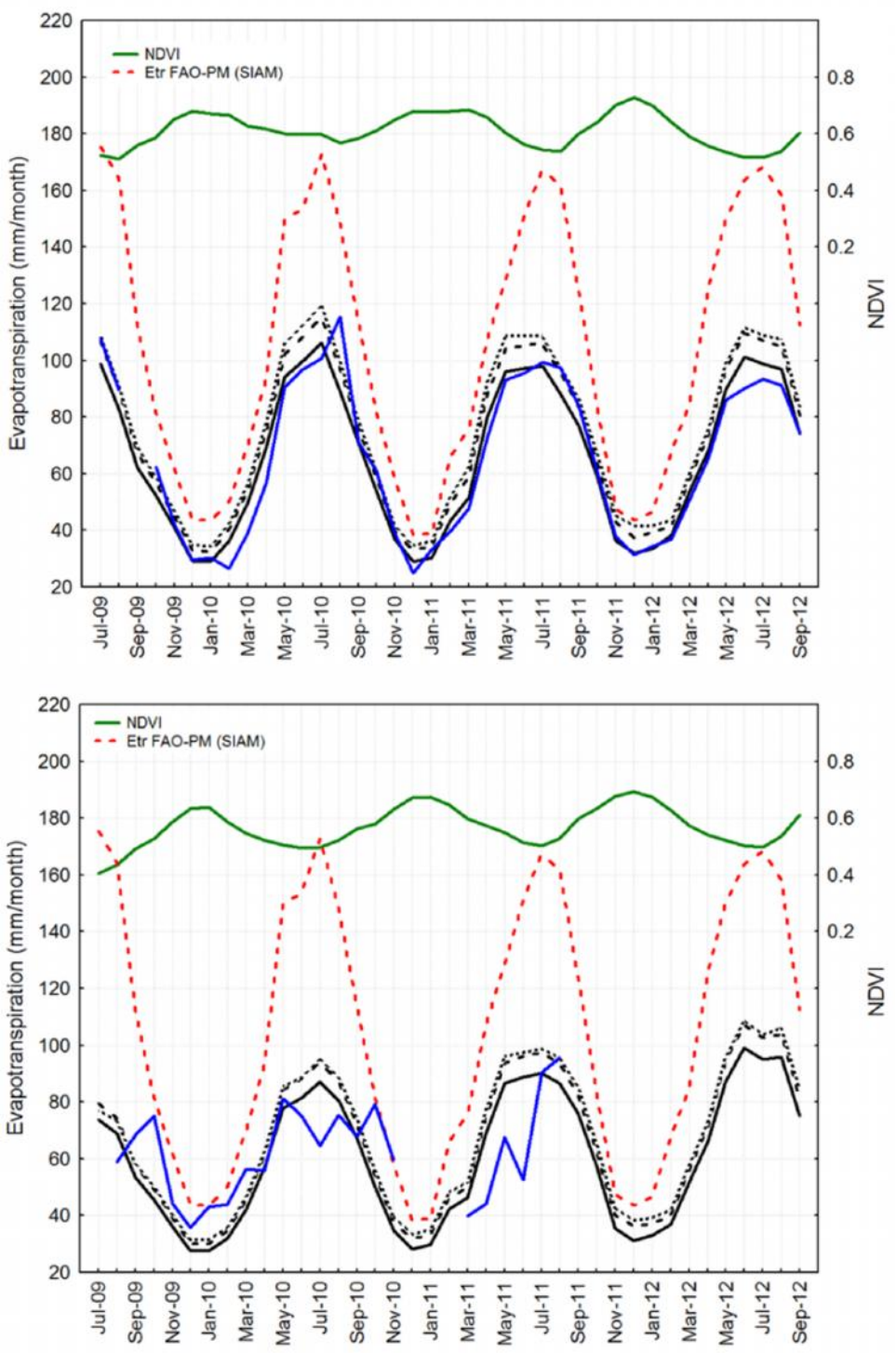

Figure 24. NDVI dynamics (green line), and reference (red line), actual (blue line) and SPHY-based (black lines) evapotranspiration values for VA (up panel) and CM (bottom panel) experimental sites. SPHY estimates are shown using the uncalibrated (dashed) and calibrated (solid) NDVI-k_c functions, and the Kamble's equation (dotted).

3.2 Sensitivity analysis

Sensitivity analysis of SPHY at Villa Antonia experimental site reveals that; 1) $k_{c,max}$ and soil depth are the most influential variables in controlling water storage in the soil bucket and its

availability for meeting the total crop water requirements, and 2) soil depth, and the beta-scalar parameter as the most important ones in generating drainage (Table 9, Figure 25 and Figure 26). In general, model results are affected in a non linear way by soil depth, beta and $NDVI_{max}$ parameters. Focusing on the soil depth as the main influential parameter in the model structure, results show differences in the outputs estimated for the Villa Antonia experimental site and those computed at the catchment scale, although trends are quite similar. At the catchment scale, the relative change accounted on the objective output variables (*eta*^{sm} and *dra*) after a relative change -RC- in soil depth can be described using an a hyperbolic function (R^2 = 0.996) and an exponential decay function (R^2 = 0.998), respectively

$$RC_{etasm} = 6.041 \cdot \frac{RC_Z}{9.133 + RC_z} - 0.3141 \cdot RC_Z + 0.7239$$

Equation 26

$$RC_{dra} = 1.800 \cdot \exp(-0.9145 \cdot RC_Z) + 0.2495$$

Equation 27

In which, RC_{etasm} and RC_{dra} are the relative changes estimated for *eta*^{sm} and *dra* respectively, and RC_Z is the relative change in soil depth.

Similarly, we extracted the function which relates the changes in the irrigation supplies required to meet the crop water requirements in the irrigated farmland area when soil depth is changed (Equation 28). It has been estimated that an increase in the active soil depth from 0.5 m to 1.0 m (or 1.5 m) will related with a reduction in irrigation requirements of 31 hm^3/año (or 45.6 hm^3/y).

$$RC_{irr} = 0.7794 \cdot \exp(-0.7464 \cdot RC_Z) + 0.6103$$

Equation 28

Here, it is important to note that sensitivity analysis was performed for assessing the potential uncertainties related within SPHY model and its parameterization. Because a no feedback has been recognized between greenness dynamics and soil moisture, among other factors, sensitivity analysis should not be used in assessing quantitatively how environmental changes could impact on the water fluxes actually simulated.

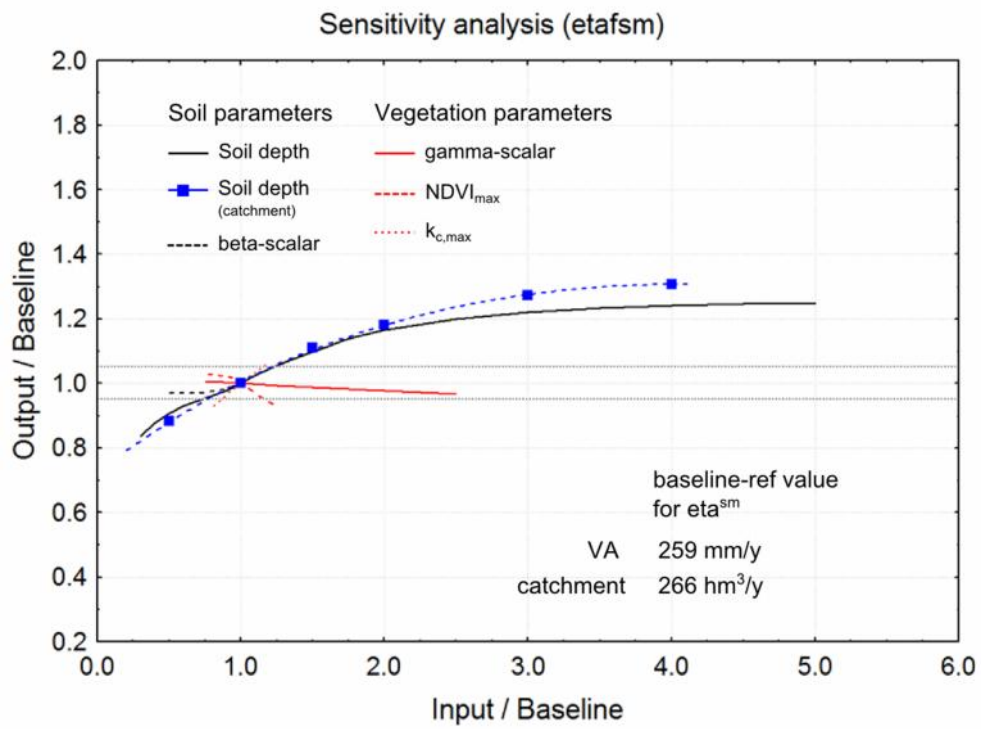

Figure 25. Relative changes in *eta*^{sm} driven by relative changes in soil and vegetation input parameters, at VA experimental site (black/red lines), and at the whole catchment (blue squares/line).

Baseline-reference values for input parameters are described in Table 9.

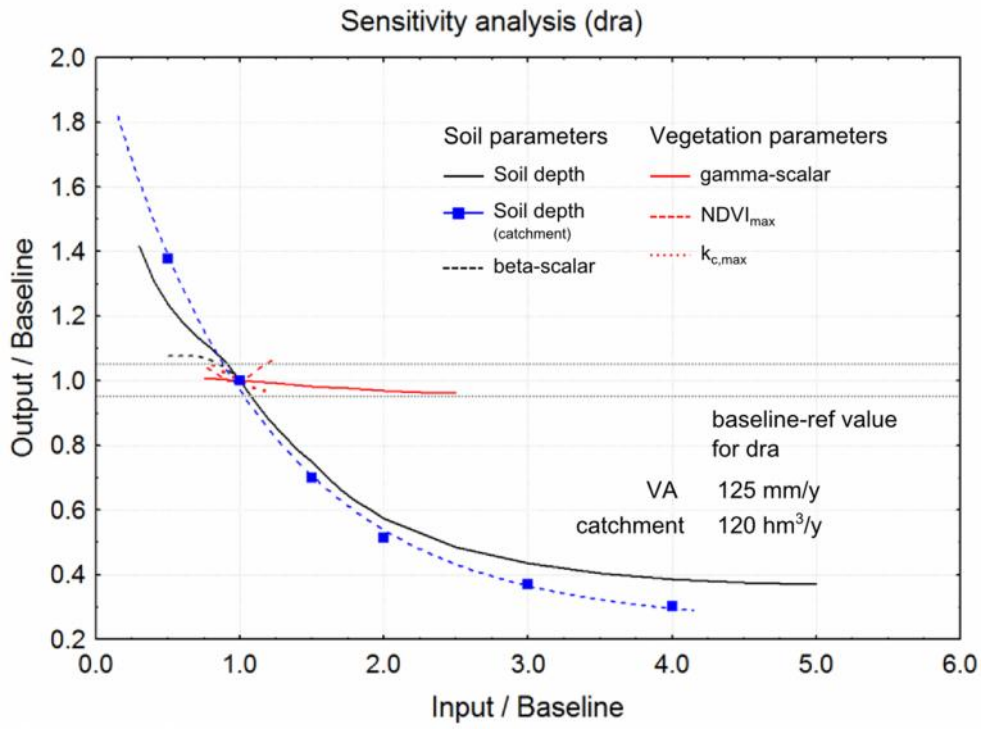

Figure 26. Relative changes in *dra* driven by relative changes in soil and vegetation input parameters, at VA experimental site (black/red lines), and at the whole catchment (blue squares/line).

Baseline-reference values for input parameters are described in Table 9.

3.3 Catchment-scale results

Annual water requirements in the irrigated area of the Campo de Cartagena basin have been estimated at around 300 hm^3/y (Table 12). This represents almost 1.4 times the total precipitation recorded in the farmland area. As it can be verified, the adoption of a dual-crop approach for the parameterization of the NDVI-k_c did not generate significant differences compared with the single NDVI-k_c equation. In this area, evapotranspiration and irrigation requirements were reduced for the study period by 1.0%, and 2.7% respectively, while total drainage (sum of surface runoff and percolation) was similar between both SPHY configurations. Despite these small differences, here the dual-crop parameterization model was retained as the best option for the WIS-CT its higher performance in *Citrus*-dominated areas without thereby large increase in the overall model complexity.

To meet the actual water requirements of crops during the study period, total irrigation inputs have been estimated at around 155±29 hm^3/y. The mean annual value of total drainage losses (runoff + percolation) reached 72.5±44.3 hm^3/y in the irrigated area, 51±34 in the non-irrigated area, and 123±77 hm^3/y for the whole basin. Maximum evapotranspiration losses are reached in April in native vegetation, but in June in the irrigated zone (Figure 27). The relative contribution of irrigation to total evapotranpiration varies along the year. In December-January, after and during the wet season, when soil moisture stored in the soil bucket is almost sufficient to meet the crop water requirements, irrigation inputs hardly meet 10% of the total requirements. Then, irrigation increases its importance up to represent in July the 100% of the total evapotranspiration (Figure 27). The total volume of drainage, considered here as potential recharge or recharge in transit to aquifers, represents an average water depth of 116 mm/y (Table 13) which was in the range of others independent and complementary soil-water balance studies performed in the region. Based on the Thornthwaite method, IGME [1994] estimated the total recharge to the unconfined aquifer in 69 hm^3/y, i.e. an areally-average figure of 61 mm/y. Jiménez-Martínez et al. [2010] estimated typical values of total recharge for the main irrigated crops in the region (rotation of lettuce-melon, artichoke, and Citrus orchards) using the VISUAL-BALAN code. From the crop-based values reported by them, total recharge in the farmland region would reach 170-190 mm/y assuming an irrigated area of 450-500 km^2. Using tracer techniques, Baudron et al. [2013] estimated an average rate of modern recharge to the unconfined aquifer of 210 mm/y.

Table 12. Mean annual values (Oct2000 – Sep2012) for the main water balance components in Campo de Cartagena agroecosystem basin. All values in hm^3/year.

Hydrological variable	Non-irrigated area	Irrigated area	
		Single-crop	Dual-crop
pre	168 ± 51	217 ± 51	
eta	110 ± 22	300 ± 12	297 ± 12
roff	4 ± 6	4 ± 9	4 ± 9
per	46 ± 29	66 ± 37	66 ± 37
irr		159 ± 29	155 ± 29

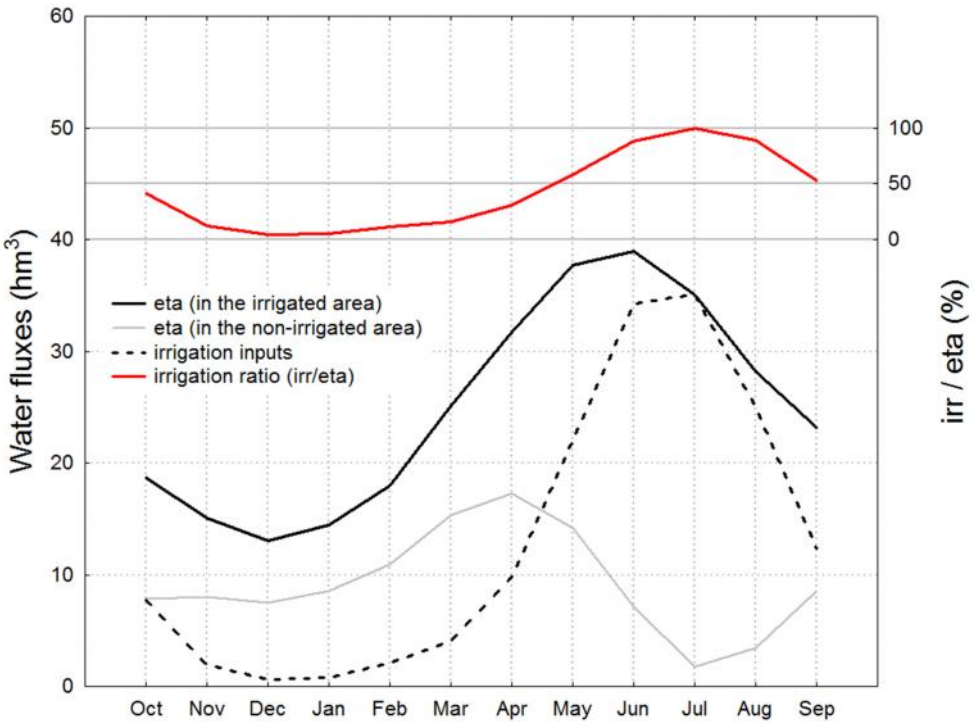

Figure 27. Average evapotranspiration (hm^3/month) estimated for irrigated and non-irrigated areas, and total irrigation inputs and percentage in relation with total evapotranspiration.

Table 13. Review of recharges estimates in the study area according different methods.

Reference	Approach	Spatial-average rate of recharge (mm/y)	Notes
IGME [1994]	Thornthwaite method	61	estimated for the unconfined aquifer
Jiménez-Martínez et al. [2010]	Crop-based estimates based on VISUAL-BALAN model	170-190	assuming an irrigated area of 450-500 km^2.
Baudron et al. [2013]	Tracer techniques	210	modern recharge
This study	SPHY model	116	potential recharge (recharge in transit)

Spatial fields of the mean annual and seasonal averages of actual evapotranspiration, total drainage, irrigation inputs are shown in Figure 28, Figure 29 and Figure 30, respectively. As it can be observed, the reliance of the basin on irrigation inputs is especially relevant during the

winter period in coincidence with the development of the winter crops (lettuce, artichoke, broccoli, and cauliflower).

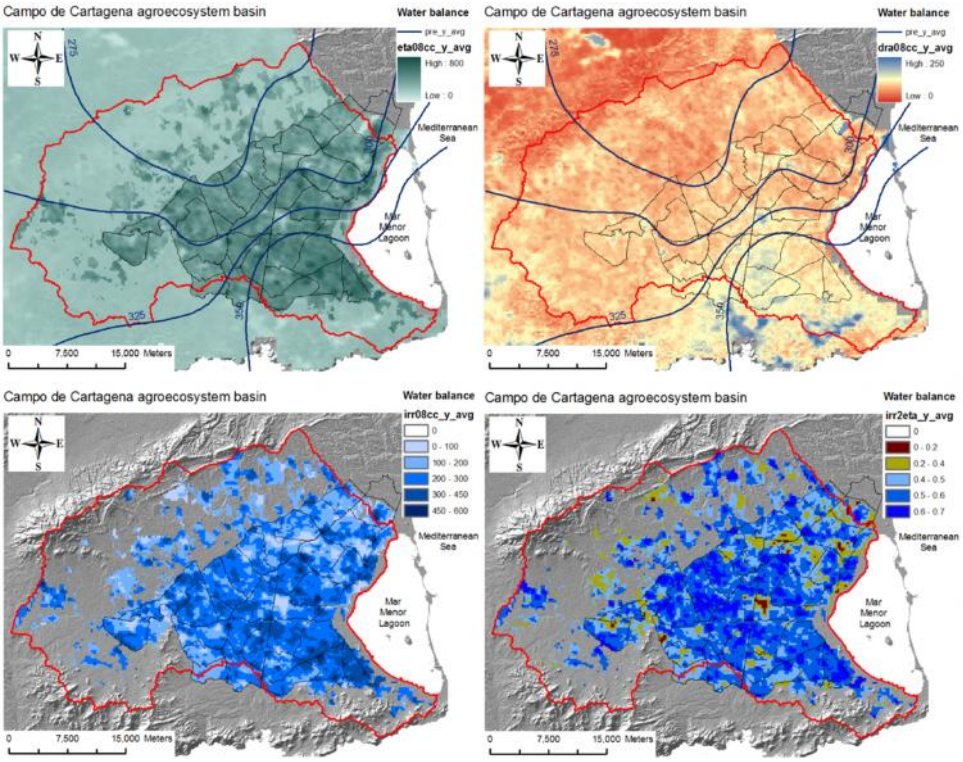

Figure 28. Mean annual values of evapotranspiration (upper left), total drainage (upper right) and irrigation (bottom left), and percentage of water depth anomaly in the non-irrigated area. All water balance components in mm.

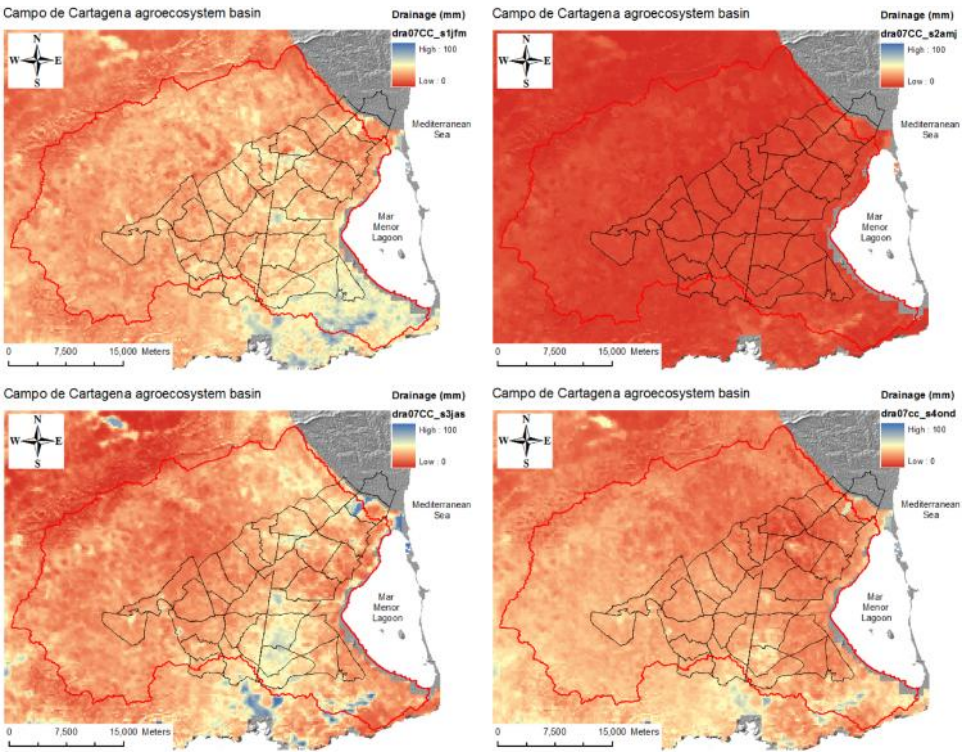

Figure 29. Seasonal variability in the total of drainage estimated by SPHY.

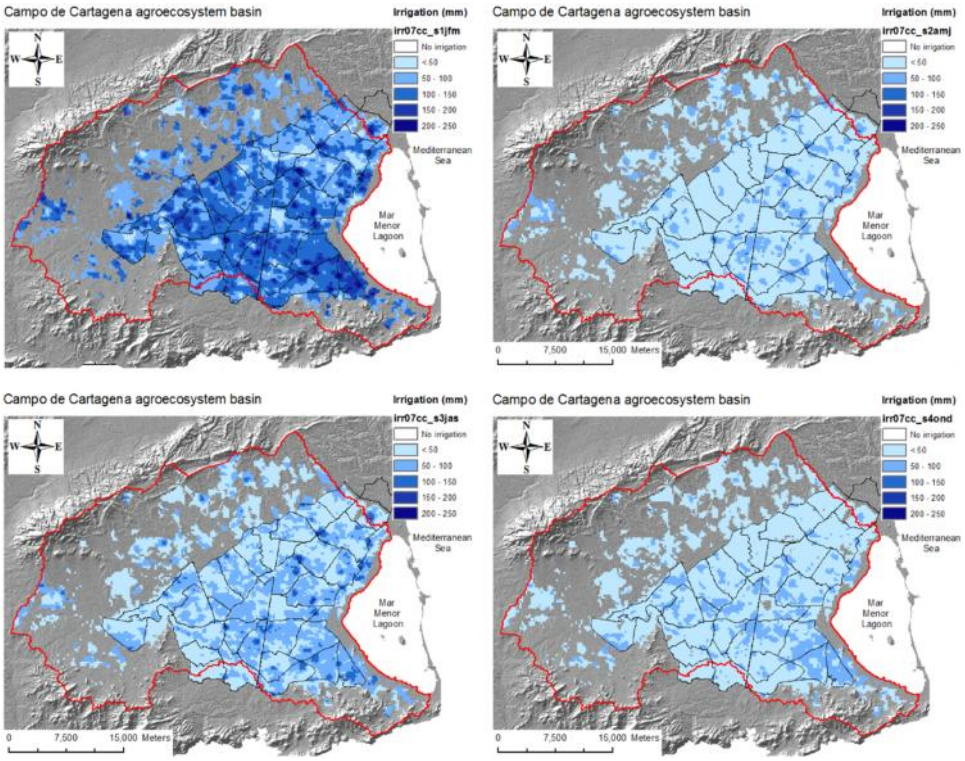

Figure 30. Seasonal variability in the total of irrigation estimated by SPHY.

3.4 Water accounting and management indicators

Water accounting diagrams summarizing the water balance components at the basin scale are shown in Figure 31, Figure 32 and Figure 33. On average, the Evapotranspiration Fraction (eta/pre) at the basin scale was 1.14, and increased up to 1.66 and decreased to 0.69 during the driest and wettest hydrological years, respectively (Table 14). Irrigation inputs to the basin reached their maxima during the 2011-2012 hydrological year (201 hm^3/y), while the lowest input rate took place during 2009-2010 (117 hm^3/y) (Figure 34). In average, 52% of the actual evapotranspiration was met by irrigation inputs during the study period, while the remaining was met by moisture stored in the soil bucket. The relative contribution of the soil moisture to the total evapotranspiration ranged between 35-70% along the study period (Figure 34). As expected, a negative relationship was found between irrigation requirements and rainfall: the drier the year, the higher the requirements of irrigation inputs to the system. During rainfall-average hydrological years, groundwater abstraction from deep confined aquifers was estimated to be similar to the total percolation recharging the unconfined aquifer, or even slightly higher if water losses along the conveyance system and a fraction of the surface runoff would had been considered. These figures may suggest, at least in average terms, that groundwater abstractions in the region are close to natural recharge. However, it is highlighted that groundwater resources are primarily pumped from the deep confined layers but not from the shallow unconfined aquifer which is receiving much of the polluted return flows resulting from the agriculture industry.

During the study period, a mean annual volume of 63 hm^3/year was delivered from the Tajo-Segura aqueduct, while 113 hm^3/year was estimated to be pumped from the groundwater system. This mean annual extraction rate was computed after the water losses by evaporation in the on-farm water reservoirs (~16 hm^3/year) were discounted [*Martínez Alvarez et al.*, 2008].

After local rainfall, groundwater is the most important source of irrigation water in the region and it plays a key role in the sustainability of the Campo de Cartagena agroecosystem (Table 14. Performance indicators at the basin scale reported at Campo de Cartagena.Table 14, Figure 35). During the driest year, when total percolation in the basin was estimated by 33 mm (20% the annual rainfall), the delivery of water from the Tajo-Segura aqueduct raised its relative contribution to the total evapotranspiration by a factor of 15 percentage points, while groundwater pumping did it by a factor of 5. Despite this, groundwater extraction was still higher than the total volume of surface water supplied from the aqueduct (121 vs 101 hm^3). As a consequence of the high rates of groundwater pumping, and the offset of the irrigation return flows and the aquifer recharge, the water balance in the groundwater system during the driest year reached very negative values (Table 14).

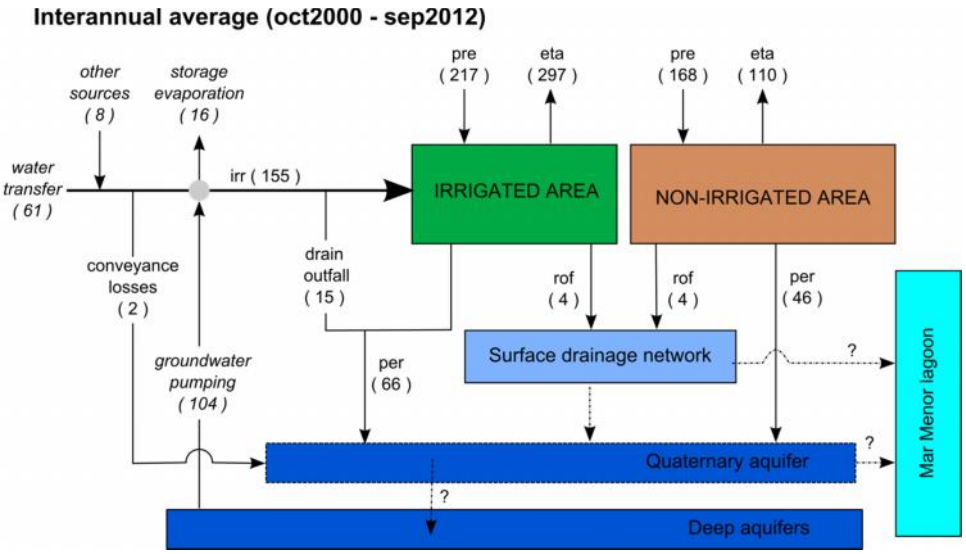

Figure 31. Water accounting diagram for the Campo de Cartagena basin. Mean annual values for the Oct2000-Sep2012 period.

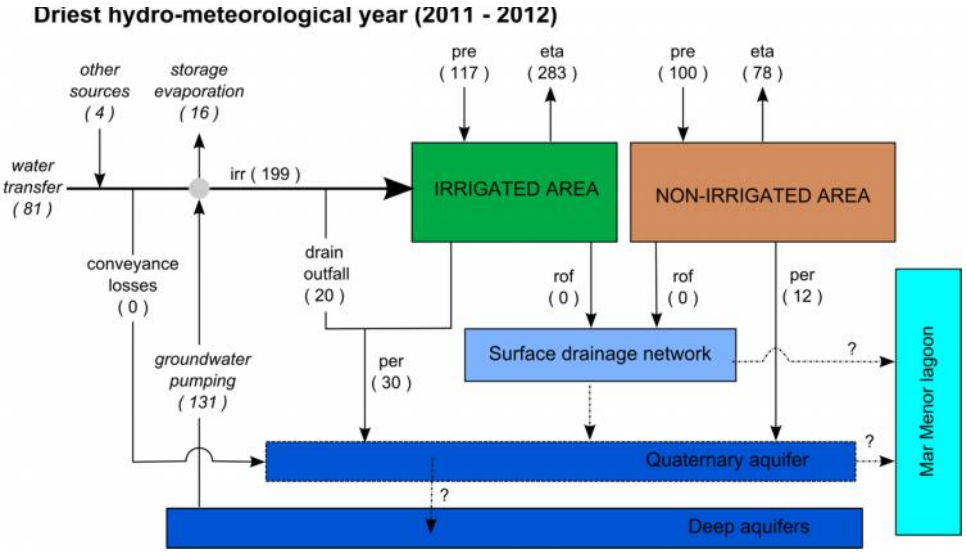

Figure 32. Water accounting diagram for the Campo de Cartagena basin during the driest hydrological year.

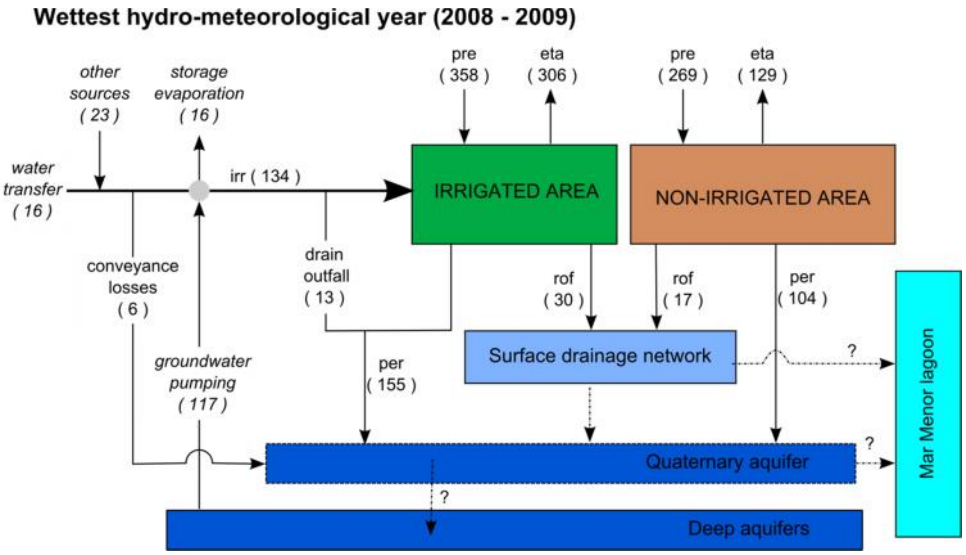

Figure 33. Water accounting diagram for the Campo de Cartagena basin during the wettest hydrological year.

Table 14. Performance indicators at the basin scale reported at Campo de Cartagena.

Performance indicator	Interann. average	Driest year (Oct2011-Sep2012)	Lowest surface water transfer year (Oct2006-Sep2007)	Wettest year (Oct2008-Sep2009)
ET fraction (eta / pre)	1.06	1.66	1.00	0.69
Groundwater abstraction intensity ratio (gwp / eta^{irr})	0.35	0.46	0.51	0.38
Groundwater system balance (per + cl – gwp) (hm^3/year)	8	-88	-12	+143
Relative irrigation supply (irr / eta^{irr})	0.52	0.70	0.52	0.44
Water transfer irigation reliance (swt / eta^{irr})	0.21	0.28	0.02	0.05

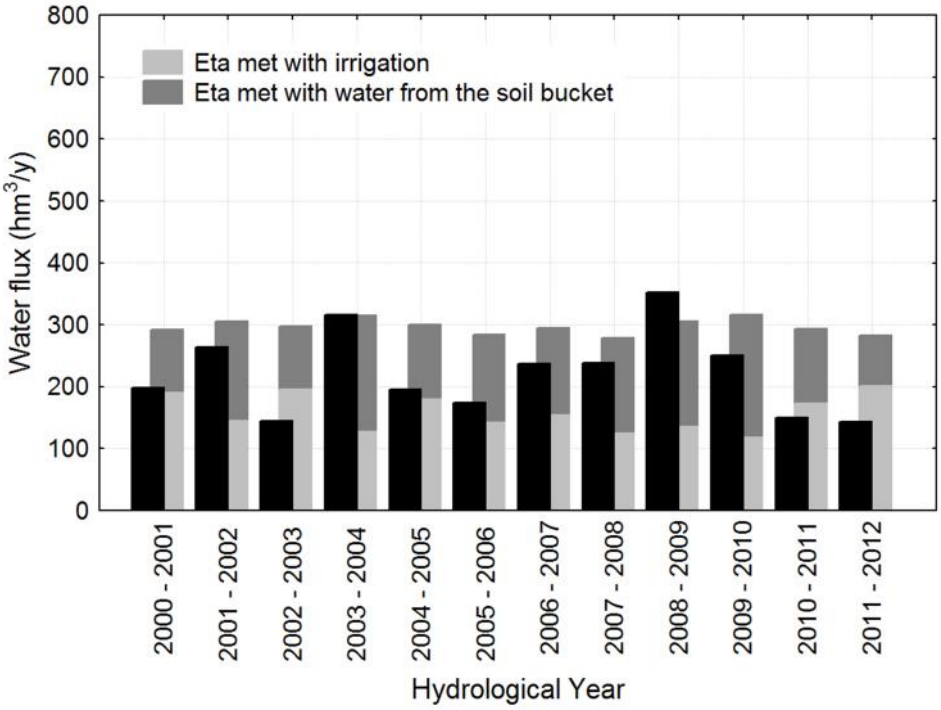

Figure 34. Interannual variability of precipitation (black bar), and total evapotranspiration in the irrigated area met by irrigation and soil moisture.

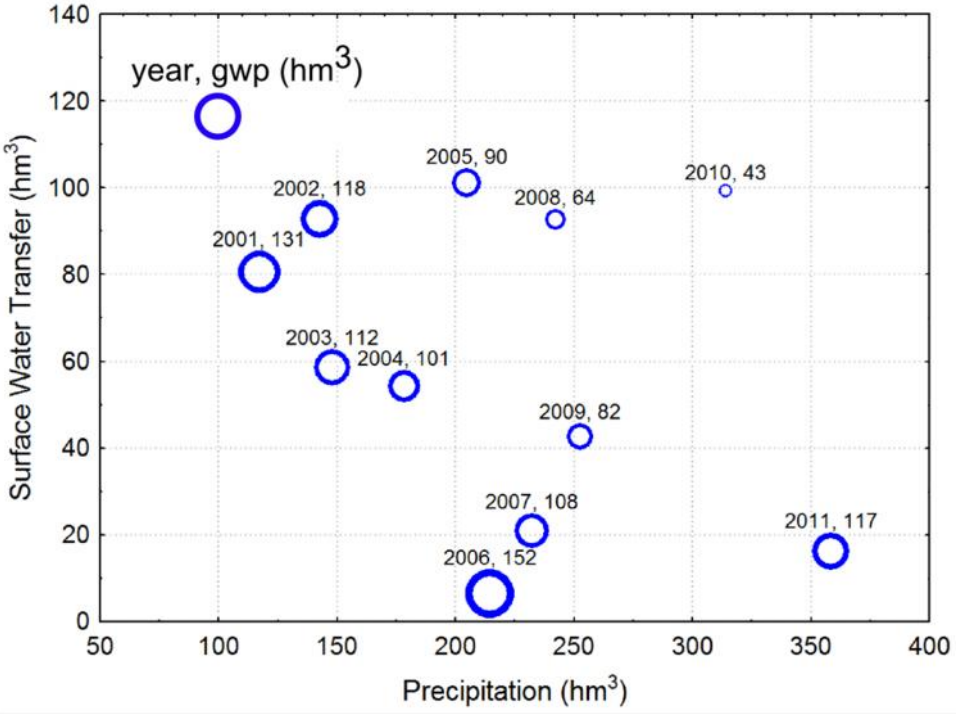

Figure 35. Annual precipitation inputs (x-axis) in the irrigated area, and water deliveries for irrigation provided from the Tajo-Segura aqueduct (y-axis) and from groundwater abstractions (bubbles with values).

Finally, average values of evapotranspiration and irrigation requirements for the Oct2000-Sep2012 period were grouped by irrigation zones in Figure 36. As it was expected, interannual variability observed for the irrigation requirements was higher than for evapotranspiration. This is because irrigation in SPHY is strongly coupled with the soil moisture dynamics and

consequently to rainfall inputs, which in semiarid regions are characterized by their strong temporal variability and stochasticity.

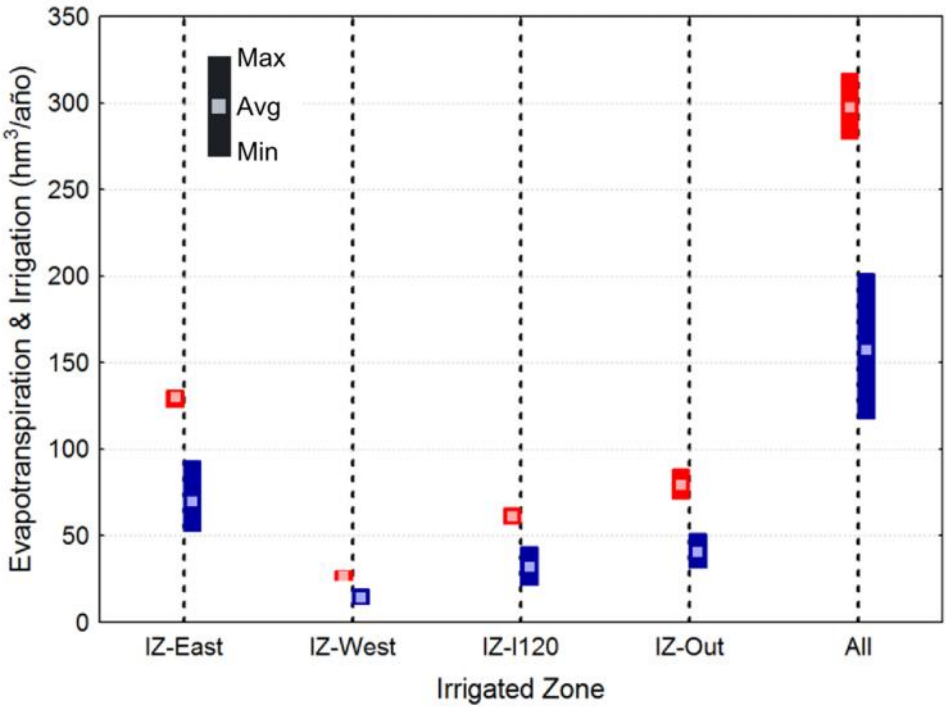

Figure 36. Mean annual evapotranspiration and irrigation inputs according Irrigated Zones (Figure 4).

3.5 Climate change scenarios

Annual reference evapotranspiration for both, A2 and B2, scenarios is expected to increase between 244 mm (19%) and 217 mm (17%) respectively against the baseline reference value observed during the control period (1276 mm/y). Higher increases are predicted during the late spring and summer months with rates of change of more than 20 mm/month (Figure 37).

Assuming the same temporal pattern of rainfall inputs, and crop coverage and greenness dynamics as for the control-baseline reference period (Oct2000 – Sep2012), the increase in the reference evapotranspiration projected for the 2090-2100 period, may promote an increase of 18-20% (53-60 hm^3/y) for the actual evapotranspiration. To cope with this future scenario of higher water requirements by crops, an extraordinary provision of water for irrigation from 48 to 54 hm^3/y should be supplied to the agrosystem. Mean annual percolation to aquifers is estimated to decrease by 5 hm^3/y against the baseline-reference value observed during the control period Table 15.

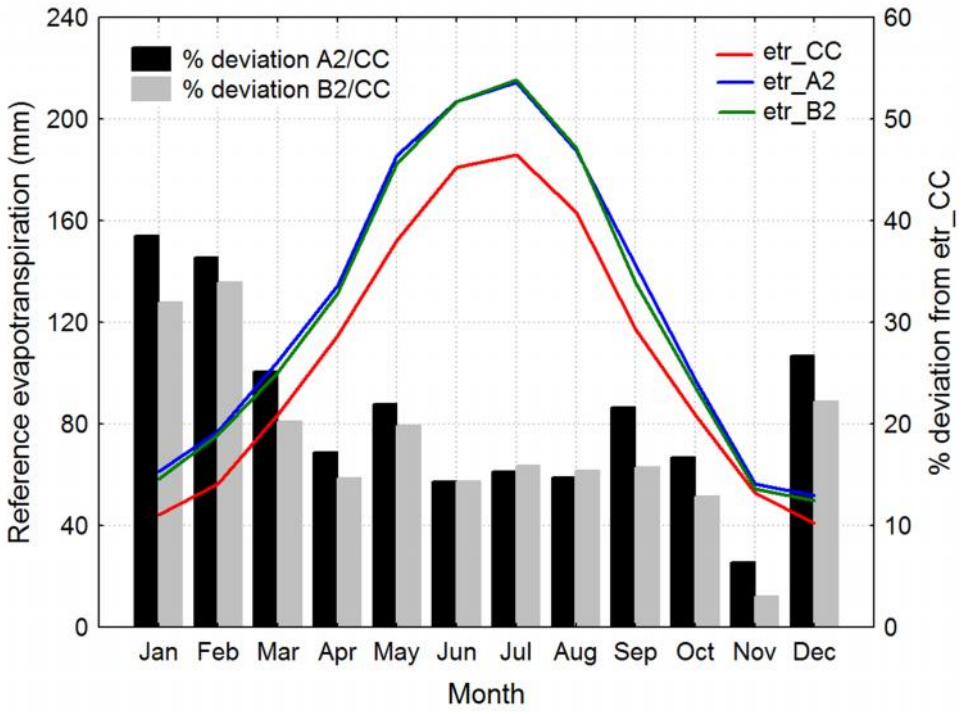

Figure 37. Average-seasonal changes in the H-S reference evapotranspiration rates for the 2091-2100 period.

Table 15. Mean annual values (± 1*SD) of the main water balance terms at the present period (Oct2000-Sep2012) and future scenarios of climate change (2090-2100).

	CC		A2		B2	
	Non-irrigated area	Irrigated area	Non-irrigated area	Irrigated area	Non-irrigated area	Irrigated area
eta	110 ± 22	297 ± 12	119 ± 26	357 ± 14	118 ± 26	350 ± 14
irr		155 ± 29		209 ± 34		203 ± 33
per	46 ± 29	66 ± 37	39 ± 25	61 ± 30	37 ± 24	63 ± 31

3.6 Online mapping tool

To make outputs of the WIS-CT accessible to the stakeholders, the *WaterMaps* web tool was used. WaterMaps is a web application that combines the functionality of *Google Maps* and the time-dependent output of water simulation models. The interface has been developed to give anyone with access to internet the possibility to explore water-related model results on the web. *WaterMap* is an undemanding visualization tool that makes it possible to set up with small effort a project-dedicated page of spatial and time variable results from hydrological models.

The WaterMap of Campo de Cartagena (WaterMap-CT) can be accessed at http://www.futurewater.nl/watermaps/wis-ct (Figure 38).

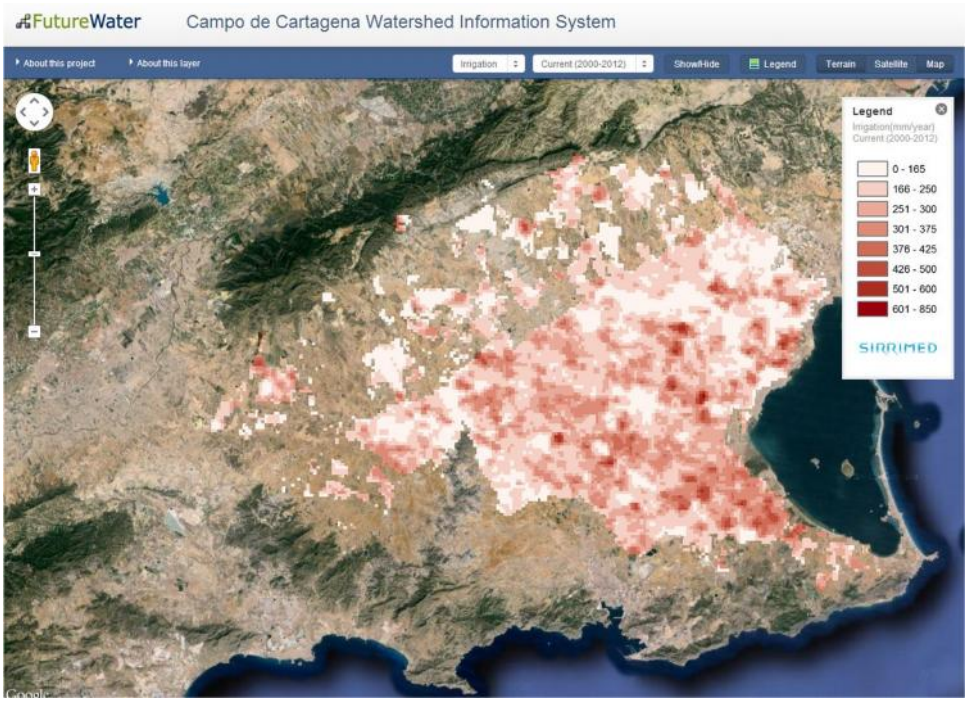

Figure 38. WaterMap web tool for the Campo de Cartagena Basin.

The main information provided by WaterMap-CT can be accessed through two tabs and two drop-down menus located in the upper section of the tool. In the first tab "*About this project*" a brief description of the SIRRIMED project and a figure with the mean water accounts in the basin are provided. The second tab "*About this layer*" gives information about the variable which is being currently displayed and how it was computed. Finally, at the center of the main panel the drop-down menus can be expanded in order to select the variable/ratio and the reference period desired by the user. Besides the annual values for each variable/ratio during the current period, layers with the annual averages values for the current period (2000-2012) and the future scenario (2070-2100) are also included. All the items available in the WaterMap-CT are shown in Figure 39, and the variables and ratios included are listed in Table 16.

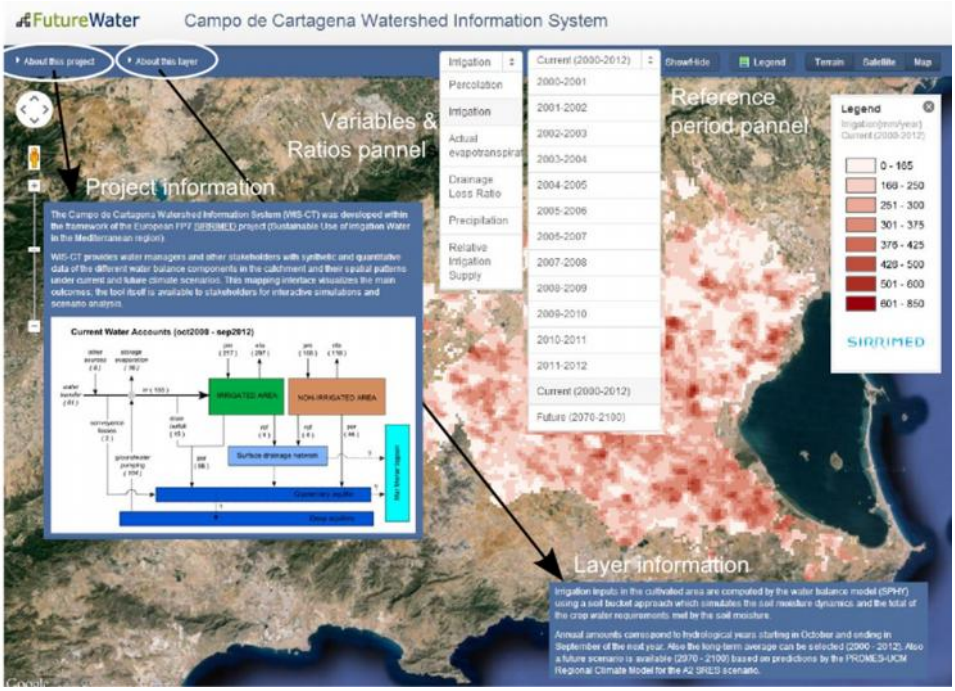

Figure 39. Items available in the WaterMap-CT.

Table 16. List of variables and ratios included in the WaterMap-CT tool.

Variable/Ratio	Unit
Precipitation (pre)	mm/y
Actual Evapotranspiration (eta)	
Irrigation (irr)	
Percolation (per)	
Drainage Loss Ratio (per+rof*)/(pre+irr)	Nondimensional
Relative Irrigation Supply (irr/eta)	

* rof = surface runoff

4 Conclusions

This report summarizes the development of a decision support tool for the Campo de Cartagena basin integrating hydrological modelling and remote sensing-data. The resulting Watershed Information System of Campo de Cartagena (WIS-CT) shows synthetic and quantitative outputs of the different water balance components at the catchment scale at a 250 m spatial resolution and on a monthly time basis.

On the watershed scale, the analysis shows that the irrigated area consumes 83% of the total water inputs into the system by precipitation, groundwater abstractions and inter-basin water transfers. In average, 52% of the total water requirements of crops is met by irrigation inputs while the remaining is provided by the moistured stored in the soil bucket. In average, the ratio between percolation losses to aquifers and groundwater abstractions at te basin scale is 0.87, although it is important to note that most of those percolation losses reach highly-polluted upper aquifers which are not being exploited at the present, while most of the groundwater abstraction pressures are focused on the deeper aquifers. Seasonally, the relative contribution of the irrigation inputs to the total water requirements of crops varies from 10% during the wet season, up to 100% in July.

The combination of SPHY model and the NDVI-based crop coefficient methodology showed to be a useful and straightforward tool for water resources assessments on this spatial and temporal scale. The outcomes were compared with field measurements and other studies and showed a good correspondence. The methodology allows to obtain insights on: a) the irrigation water inputs provided to crops when these information is not available, and b) the surface and groundwater interactions accounted in very heterogeneous irrigated agroecosystems.

Overall, the outcomes lead to a better understanding of the water balance of this semiarid Mediterranean basin with intensive irrigated agriculture. The information is made accessible for water managers and other stakeholders through a web mapping tool.

5 References

Allen, R. G., L. S. Pereira, D. Raes, and M. Smith (1998), *Crop evapotranspiration, FAO technical report num. 56*, Rome.

Baudron, P., F. Barbecot, J. L. G. Aróstegui, C. Leduc, Y. Travi, and D. Martinez-Vicente (2013), Impacts of human activities on recharge in a multilayered semiarid aquifer (Campo de Cartagena, SE Spain), *Hydrol. Process.*, 2223–2236, doi:10.1002/hyp.9771.

Brunet, M., M. De Castro, E. Petisco, P. Ramos, J. Ribalaygua, I. Sanz, and L. Torres (2009), *Generación de escenarios regionalizados de cambio climático para España*, Madrid.

Campos, I., J. Villodre, A. Carrara, and A. Calera (2013), Remote sensing-based soil water balance to estimate Mediterranean holm oak savanna (dehesa) evapotranspiration under water stress conditions, *J. Hydrol.*, *494*, 1–9, doi:10.1016/j.jhydrol.2013.04.033.

Cantón, Y., A. Solé-Benet, J. de Vente, C. Boix-Fayos, A. Calvo-Cases, C. Asensio, and J. Puigdefábregas (2011), A review of runoff generation and soil erosion across scales in semiarid south-eastern Spain, *J. Arid Environ.*, *75*(12), 1254–1261, doi:10.1016/j.jaridenv.2011.03.004.

Carlson, T. N., and D. A. Riziley (1997), On the relation between NDVI , Fractional Vegetation Cover, and Leaf Area Index, *Remote Sens. Environ.*, *62*, 241–252, doi:http://dx.doi.org/10.1016/S0034-4257(97)00104-1.

Chen, J., P. Jönsson, M. Tamura, Z. Gu, B. Matsushita, and L. Eklundh (2004), A simple method for reconstructing a high-quality NDVI time-series data set based on the Savitzky–Golay filter, *Remote Sens. Environ.*, *91*(3-4), 332–344, doi:10.1016/j.rse.2004.03.014.

Contreras, S., M. M. Boer, F. J. Alcalá, F. Domingo, M. García, A. Pulido-Bosch, and J. Puigdefábregas (2008), An ecohydrological modelling approach for assessing long-term recharge rates in semiarid karstic landscapes, *J. Hydrol.*, *351*(1-2), 42–57, doi:10.1016/j.jhydrol.2007.11.039.

Contreras, S., E. G. Jobbágy, P. E. Villagra, M. D. Nosetto, and J. Puigdefábregas (2011), Remote sensing estimates of supplementary water consumption by arid ecosystems of central Argentina, *J. Hydrol.*, *397*(1-2), 10–22, doi:10.1016/j.jhydrol.2010.11.014.

Van Dam, O. (2000), *Modelling incoming potential radiation on a land surface with PCRaster: POTRAD5.MOD manual*, Utrech Centre for Environment and Landscape Dynamics, Utrecht University, Utrecht.

Descheemaeker, K., D. Raes, R. Allen, J. Nyssen, J. Poesen, B. Muys, M. Haile, and J. Deckers (2011), Two rapid appraisals of FAO-56 crop coefficients for semiarid natural vegetation of the northern Ethiopian highlands, *J. Arid Environ.*, *75*(4), 353–359, doi:10.1016/j.jaridenv.2010.12.002.

Descroix, L., D. Viramontes, J. Estrada, J.-L. Gonzalez Barrios, and J. Asseline (2007), Investigating the spatial and temporal boundaries of Hortonian and Hewlettian runoff in Northern Mexico, *J. Hydrol.*, *346*(3-4), 144–158, doi:10.1016/j.jhydrol.2007.09.009.

Er-Raki, S., A. Chehbouni, N. Guemouria, B. Duchemin, J. Ezzahar, and R. Hadria (2007), Combining FAO-56 model and ground-based remote sensing to estimate water

consumptions of wheat crops in a semi-arid region, *Agric. Water Manag.*, *87*(1), 41–54, doi:10.1016/j.agwat.2006.02.004.

Fernandez-Illescas, C. P., A. Porporato, F. Laio, and I. Rodriguez-Iturbe (2001), The ecohydrological role of soil texture in a water-limited ecosystem, *Water Resour. Res.*, *37*(12), 2863–2872, doi:10.1029/2000WR000121.

Finch, J. W. (1998), Estimating direct groundwater recharge using a simple water balance model – sensitivity to land surface parameters, *J. Hydrol.*, *211*(1-4), 112–125, doi:10.1016/S0022-1694(98)00225-X.

Glenn, E. P., C. M. U. Neale, D. J. Hunsaker, and P. L. Nagler (2011), Vegetation index-based crop coefficients to estimate evapotranspiration by remote sensing in agricultural and natural ecosystems, *Hydrol. Process.*, *25*(26), 4050–4062, doi:10.1002/hyp.8392.

González-Dugo, M. P., and L. Mateos (2008), Spectral vegetation indices for benchmarking water productivity of irrigated cotton and sugarbeet crops, *Agric. Water Manag.*, *95*(1), 48–58, doi:10.1016/j.agwat.2007.09.001.

Groeneveld, D. P., W. M. Baugh, J. S. Sanderson, and D. J. Cooper (2007), Annual groundwater evapotranspiration mapped from single satellite scenes, *J. Hydrol.*, *344*(1-2), 146–156, doi:10.1016/j.jhydrol.2007.07.002.

Hollis, J. M., J. Hannam, and P. H. Bellamy (2012), Empirically-derived pedotransfer functions for predicting bulk density in European soils, *Eur. J. Soil Sci.*, *63*(1), 96–109, doi:10.1111/j.1365-2389.2011.01412.x.

IGME (1994), *Las aguas subterráneas del Campo de Cartagena*, Madrid.

IPCC (2000), *Emissions Scenarios. A Special Report of Working Group II of the Intergovernmental Panel on Climate Change*, edited by N. Nakicenovic and R. Swart, Cambridge University Press, Cambridge.

Jayanthi, H., C. M. U. Neale, and J. L. Wright (2007), Development and validation of canopy reflectance-based crop coefficient for potato, *Agric. Water Manag.*, *88*(1-3), 235–246, doi:10.1016/j.agwat.2006.10.020.

Jiménez-Martínez, J., T. H. Skaggs, M. T. van Genuchten, and L. Candela (2009), A root zone modelling approach to estimating groundwater recharge from irrigated areas, *J. Hydrol.*, *367*(1-2), 138–149, doi:10.1016/j.jhydrol.2009.01.002.

Jiménez-Martínez, J., L. Candela, J. Molinero, and K. Tamoh (2010), Groundwater recharge in irrigated semi-arid areas: quantitative hydrological modelling and sensitivity analysis, *Hydrogeol. J.*, *18*(8), 1811–1824, doi:10.1007/s10040-010-0658-1.

Jiménez-Martínez, J., L. Candela, J. L. García-Aróstegui, and R. Aragón (2012), A 3D geological model of Campo de Cartagena, SE Spain: Hydrogeological implications, *Geol. Acta*, *10*(1), 49–62, doi:10.1344/105.000001703.

Jönsson, P., and L. Eklundh (2002), Seasonality Extraction by Function Fitting to Time-Series of Satellite Sensor Data, *IEEE Trans. Geosci. Remote Sens.*, *40*(8), 1824–1832, doi:10.1109/TGRS.2002.802519.

Jönsson, P., and L. Eklundh (2004), TIMESAT—a program for analyzing time-series of satellite sensor data, *Comput. Geosci.*, *30*(8), 833–845, doi:10.1016/j.cageo.2004.05.006.

Kamble, B., A. Irmak, and K. Hubbard (2013), Estimating Crop Coefficients Using Remote Sensing-Based Vegetation Index, *Remote Sens.*, *5*(4), 1588–1602, doi:10.3390/rs5041588.

Karimi, P., W. G. M. Bastiaanssen, and D. Molden (2013), Water Accounting Plus (WA+) – a water accounting procedure for complex river basins based on satellite measurements, *Hydrol. Earth Syst. Sci.*, *17*(7), 2459–2472, doi:10.5194/hess-17-2459-2013.

Kendy, E., P. Gerard-Marchant, M. Todd Walter, Y. Zhang, C. Liu, and T. S. Steenhuis (2003), A soil-water-balance approach to quantify groundwater recharge from irrigated cropland in the North China Plain, *Hydrol. Process.*, *17*(10), 2011–2031, doi:10.1002/hyp.1240.

Krause, P., D. P. Boyle, and F. Bäse (2005), Comparison of different efficiency criteria for hydrological model assessment, *Adv. Geosci.*, *5*, 89–97, doi:10.5194/adgeo-5-89-2005.

Laio, F., A. Porporato, L. Ridolfi, and I. Rodriguez-iturbe (2001), Plants in water-controlled ecosystems : active role in hydrologic processes and response to water stress II . Probabilistic soil moisture dynamics, *Adv. Water Resour.*, *24*(7), 707–723, doi:10.1016/S0309-1708(01)00005-7.

Legates, D. R., and G. J. McCabe Jr. (1999), Evaluating the use of “goodness-of-fit” measures in hydrologic and hydroclimatic model validation, *Water Resour. Res.*, *35*(1), 233–241, doi:10.1029/1998WR900018.

Martínez Alvarez, V., M. M. González-Real, a. Baille, J. F. Maestre Valero, and B. Gallego Elvira (2008), Regional assessment of evaporation from agricultural irrigation reservoirs in a semiarid climate, *Agric. Water Manag.*, *95*(9), 1056–1066, doi:10.1016/j.agwat.2008.04.003.

Molden, D., and R. Sakthivadivel (1999), Water accounting to assess use and productivity of water, *Int. J. Water Resour. Dev.*, *15*(1-2), 55–71, doi:10.1080/07900629948934.

Mutiibwa, D., and S. Irmak (2013), AVHRR-NDVI-based crop coefficients for analyzing long-term trends in evapotranspiration in relation to changing climate in the U.S. High Plains, *Water Resour. Res.*, *49*(1), 231–244, doi:10.1029/2012WR012591.

Muzylo, a., P. Llorens, F. Valente, J. J. Keizer, F. Domingo, and J. H. C. Gash (2009), A review of rainfall interception modelling, *J. Hydrol.*, *370*(1-4), 191–206, doi:10.1016/j.jhydrol.2009.02.058.

Naoum, S., and I. K. Tsanis (2003), Temporal and spatial variation of annual rainfall on the island of Crete, Greece, *Hydrol. Process.*, *17*(10), 1899–1922, doi:10.1002/hyp.1217.

Pérez-Cutillas, P. (2013), Modelización de propiedades físicas del suelo a escala regional. Casos de estudio en el Sureste Ibérico, Universidad de Murcia.

Perez-Hoyos, A., F. J. Garcia-Haro, and N. Valcarcel (2014), Incorporating Sub-Dominant Classes in the Accuracy Assessment of Large-Area Land Cover Products: Application to GlobCover, MODISLC, GLC2000 and CORINE in Spain, *IEEE J. Sel. Top. Appl. Earth Obs. Remote Sens.*, *7*(1), 187–205, doi:10.1109/JSTARS.2013.2258659.

Ramos-Calzado, P., J. Gómez-Camacho, F. Pérez-Bernal, and M. F. Pita-López (2008), A novel approach to precipitation series completion in climatological datasets : application to Andalusia, *Int. J. Climatol.*, *28*, 1525–1534, doi:10.1002/joc.

Samani, Z., A. S. Bawazir, M. Bleiweiss, R. Skaggs, J. Longworth, V. D. Tran, and A. Pinon (2009), Using remote sensing to evaluate the spatial variability of evapotranspiration and

crop coefficient in the lower Rio Grande Valley, New Mexico, *Irrig. Sci.*, *28*(1), 93–100, doi:10.1007/s00271-009-0178-8.

Sánchez, E., C. Gallardo, M. a. Gaertner, a. Arribas, and M. Castro (2004), Future climate extreme events in the Mediterranean simulated by a regional climate model: a first approach, *Glob. Planet. Change*, *44*(1-4), 163–180, doi:10.1016/j.gloplacha.2004.06.010.

Sánchez, N., J. Martínez-Fernández, J. González-Piqueras, M. P. González-Dugo, G. Baroncini-Turrichia, E. Torres, A. Calera, and C. Pérez-Gutiérrez (2012), Water balance at plot scale for soil moisture estimation using vegetation parameters, *Agric. For. Meteorol.*, *166-167*, 1–9, doi:10.1016/j.agrformet.2012.07.005.

Singh, R., and A. Irmak (2009), Estimation of Crop Coefficients Using Satellite Remote Sensing, *J. Irrig. Drain. Eng.*, *135*(5), 597–608, doi:10.1061/(ASCE)IR.1943-4774.0000052.

SIRRIMED (2012), *D4.4 and D4.5 Report on adaptations of the models and on the coupling of the crop model and hydraulic model*.

Solano, R., K. Didan, A. Jacobson, and A. Huete (2010), *MODIS vegetation indices (MOD13) C5 - User's guide*, Tucson.

Terink, W., P. Droogers, W. Immerzeel, and G. v. d. Eertwegh (2012), *SPHY – Een hydrologisch model gericht op de berekening van bodemvocht in de wortelzone en de actuele verdamping*, Wageningen, The Netherlands.

Villalobos, F. J., F. Orgaz, and E. Fereres (2006), *Estudio sobre las necesidades de agua de riego de los cultivos en la zona del trasvase Tajo-Segura*, Murcia.

Wösten, J. H. M., Y. . Pachepsky, and W. J. Rawls (2001), Pedotransfer functions: bridging the gap between available basic soil data and missing soil hydraulic characteristics, *J. Hydrol.*, *251*(3-4), 123–150, doi:10.1016/S0022-1694(01)00464-4.